**Title**
OPTICAL DETECTION OF NUCLEAR QUADRIPOLE INTERACTIONS IN EXCITED TRIPLET STATES



**Authors**
Harris, Charles B.
Buckley, Michael J.

**Publication Date**
1975-02-01

To be published as a Chapter in "Advances in Nuclear Quadrupole Resonance," Vol. II, Heyden and Son, London

LBL-3716
c.1

# OPTICAL DETECTION OF NUCLEAR QUADRUPOLE INTERACTIONS IN EXCITED TRIPLET STATES

Charles B. Harris and Michael J. Buckley



February 1975

Prepared for the U. S. Energy Research and Development Administration under Contract W-7405-ENG-48



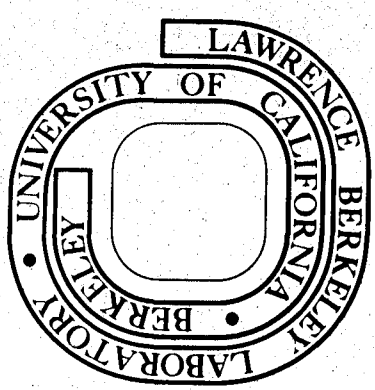


LBL-3716
c.1

## DISCLAIMER

BOOK CHAPTER: Advances in Nuclear Quadrupole Resonance, Vol. II (pub. Heyden and Son, London).

LBL-3716

# OPTICAL DETECTION OF NUCLEAR QUADRUPOLE INTERACTIONS IN EXCITED TRIPLET STATES

Charles B. Harris
Department of Chemistry, and Inorganic Materials Research Division
of Lawrence Berkeley Laboratory, University of California
Berkeley, California, USA 94720

and

Michael J. Buckley
Air Force Materials Laboratory
Wright-Patterson Air Force Base
Dayton, Ohio, USA 45433

## I. Introduction

The measurement of nuclear quadrupole coupling constants in the excited triplet state of organic molecules has only recently been possible with the development of optically detected magnetic resonance (ODMR) techniques for observing electron spin transitions in zero field. Since this technique is highly dependent on the nature of the triplet state, a short review of some of the important properties of the triplet state are given. There are several good review articles[1-3] on the triplet state to which the reader is referred for a more complete discussion. The historical development of ODMR and a survey of experimental results is then given, followed by a section that deals with the sensitivity of ODMR and optically detected ENDOR in the framework of intramolecular energy transfer processes. Specifically, the effects of radiationless, radiative, and spin-lattice relaxation processes on the overall sensitivity of ODMR are considered explicitly. The remainder of this chapter deals with the form of the spin Hamiltonian in zero-field followed by an analysis of the excited $\pi\pi^*$ triplet states of 8-chloroquinoline and paradichlorobenzene.

### A. The Excited Triplet State in Organic Molecules

The ground state of most organic molecules consists of a singlet electron configuration in which all the electrons have their spins paired. The molecule may be excited to a higher energy electron configuration by the application of electromagnetic radiation of the appropriate energy.

We will primarily be concerned with the excited electron configurations produced when one electron in the highest bonding molecular orbital ($\phi_A$) is promoted to the lowest antibonding molecular orbital ($\phi_B$). Since electrons have a spin of ½, there are four possible orientations for the two unpaired electrons, which, if we let α equal spin up and β equal spin down, may be represented as,

$$\begin{aligned} &\alpha(1)\ \alpha(2) && S_z = 1 && S^2 = 1 \\ &\alpha(1)\ \beta(2) && S_z = 0 && S^2 = 0 \\ &\beta(1)\ \alpha(2) && S_z = 0 && S^2 = 0 \\ &\beta(1)\ \beta(2) && S_z = -1 && S^2 = 1 \end{aligned} \qquad (1)$$

This representation, however, is not satisfactory since the electrons obey Fermi-Dirac statistics and thus the total wave function (orbital times spin) must be antisymmetric with respect to electron exchange. In addition, we would like the spin functions to be eigenstates of $S^2$ and $S_z$. The spin functions $\alpha(1)\ \alpha(2)$ and $\beta(1)\ \beta(2)$ are clearly eigenstates of $S^2$ and $S_z$ since $S^2 = 1$ for both and $S_z = +1$ and $-1$ respectively. We can generate the $S_z = 0$ component of the triplet spin state by applying the lowering operator to the $\alpha(1)\ \alpha(2)$ state which gives us the desired spin function,

$$^3\psi_o = [1/\sqrt{2}][\alpha(1)\ \beta(2) + \beta(1)\ \alpha(2)] \qquad (2)$$

The remaining spin function is a singlet

$$^1\psi = [1/\sqrt{2}][\alpha(1)\ \beta(2) - \beta(1)\ \alpha(2)] \qquad (3)$$

and, in contrast to the triplet spin functions, is antisymmetric with respect to electron exchange. The spatial part of the excited state

electron wavefunction may be represented as a symmetric (+) and antisymmetric (-) linear combination of $\phi_A$ and $\phi_B$ as:

$$\Psi_{\pm} = [1/\sqrt{2}][\phi_A(1)\ \phi_B(2) \pm \phi_A(2)\ \phi_B(1)] \tag{4}$$

Since the total wavefunction must be antisymmetric, there are only four allowed representations of the total wavefunction; a singlet state with a symmetric spatial function and an antisymmetric spin function,

$$^1\underline{\Psi} = [1/\sqrt{2}][\phi_A(1)\phi_B(2)+\phi_A(2)\phi_B(1)]\ [1/\sqrt{2}][\alpha(1)\ \alpha(2)-\beta(1)\beta(2)] \tag{5}$$

and a triplet state with an antisymmetric spatial function and a symmetric spin function

$$^3\underline{\Psi} = [1/\sqrt{2}][\phi_A(1)\phi_B(2) - \phi_A(2)\phi_B(1)] \cdot \begin{Bmatrix} \alpha(1)\ \alpha(2) \\ [1/\sqrt{2}][\alpha(1)\ \beta(2) + \beta(1)\ \alpha(2)] \\ \beta(1)\ \beta(2) \end{Bmatrix} \tag{6}$$

The repulsive electrostatic interaction between the two unpaired electrons gives rise to a term in the total Hamiltonian equal to $e^2/r_{12}$, where e is the electron charge and $r_{12}$ is the vector connecting the two electrons. This term removes the degeneracy of the singlet and triplet states and results in the singlet state going to higher energy while the triplet state is shifted to lower energy with an energy separation between the two states of

$$^1E - {}^3E = 2\delta_{12} \tag{7}$$

where $\delta_{12}$ is the exchange integral given by

$$\delta_{12} = \langle\phi_A(1)\phi_B(2)\ |e^2/r_{12}|\ \phi_A(2)\phi_B(1)\rangle \tag{8}$$

For most organic molecules $2\ \delta_{12}$ is 1000 to 10000 $cm^{-1}$. As we will see in the discussion of the spin Hamiltonian, the inclusion of the electron dipole-dipole interaction removes the three fold degeneracy of

the triplet state. This splitting is usually referred to as the zero field splitting and is on the order of 0.1 $cm^{-1}$. An additional contribution to the zero field splitting arises from the coupling of the spin and orbital electron angular momentum and is of the form $A(L \cdot S)$ where L and S are the spin and oribital angular momentum quantum numbers and A is a constant that depends on the particular molecule being considered. The effect of the spin-orbit Hamiltonian is to mix states of different multiplicity and, therefore, to give singlet character to triplet states and vice versa. The most important consequence of this is to permit the triplet state to undergo weak electric dipole radiation to the ground state (phosphorescence), the intensity and polarization from each of the three triplet sublevels being a function of the spin-orbit coupling to both the excited and ground singlet states.

Since the sensitivity of ODMR depends upon the number of molecules in their triplet state, an important consideration is intramolecular energy transfer processes. Following excitation, a molecule may lose energy by radiative or non-radiative pathways. Phosphorescence ($T_1 \rightarrow S_o$) and fluorescence ($S_1 \rightarrow S_o$) comprise the radiative pathways and proceed with rate constants on the order of $10^4$ to $10^{-2}$ $sec^{-1}$ and $10^6$ to $10^9$ $sec^{-1}$, respectively. The longer lifetime for phosphorescence results from the fact that the triplet state is spin-forbidden in first order for electric dipole radiation to the ground state. The molecules may also lose energy through three non-radiative pathways:

1) Vibrational Relaxation -- or passage from a non-equilibrium vibrational energy distribution in a given electronic state to the Boltzmann energy distribution relative to the zero point energy of that same state. This proceeds primarily by a non-radiative mechanism with a rate constant of approximately $10^{12}$ $sec^{-1}$.

2) Internal Conversion -- or radiationless passage between two electronic states of the same spin multiplicity. This pathway also has a fast rate constant of approximately $10^{12}$ $sec^{-1}$.

3) Intersystem Crossing -- or radiationless passage from an electronic state in the singlet manifold to an electronic state in the triplet manifold or vice versa. This pathway is slower than the other two and is on the order of $10^{4}$ to $10^{12}$ $sec^{-1}$.

Although the exact mechanisms of intersystem crossing have not been completely elucidated, it is generally found that at liquid helium temperatures (4.2°K) *the individual triplet spin sublevels of the lowest triplet states have unequal populations because of unequal intersystem crossing rates into the individual magnetic sublevels via spin orbit and spin-vibronic coupling and unequal depopulating rates.* Consequently, a state of spin alignment exists for the electron spins.[4] The various rate constants for energy transfer, the existence of spin alignment, and the spin lattice relaxation rate between the triplet spin sublevels are all important factors in determining the sensitivity of ODMR.

B. The Historical Development of ODMR

The development of any field of science is difficult to trace since every advancement is dependent on the work of many previous researchers; however, we will choose for the starting point of this discussion the extensive study of the phosphorescence of organic molecules by Lewis and Kasha[5,6] in 1944. In their series of papers it was proposed that the phosphorescent state of these molecules corresponded to their lowest triplet state. This hypothesis was strongly supported shortly thereafter by magnetic susceptibility measurements[7,8] which showed that small changes in the susceptibility were observed upon irradiation of the samples.

As with any major change in the existing paradigm of science, this hypothesis was not universally accepted.[9] The most distressing aspect of the hypothesis was the failure to observe the predicted electron spin resonance (ESR) of the phosphorescent state. The problem was resolved in 1958 when Hutchinson and Mangum[10,11] succeeded in observing the ESR of naphthalene in its phosphorescent state and showed conclusively that the phosphorescent state was a triplet state. The experiment was performed on a single crystal of naphthalene doped in durene using conventional techniques in which the absorption of the microwave energy was monitored while varying the applied magnetic field. Subsequently, the triplet state ESR of many organic compounds was observed; however, most of the work was done on randomly oriented samples. Since only one parameter can usually be measured with randomly oriented samples, the separation of the three levels of the triplet cannot be determined. In certain cases[12,13]

the three levels can be assigned but the assignment is difficult and the method has not been used often. The limited sensitivity of ESR and the difficulty of preparing single crystal samples has restricted the number of molecules investigated. Only a few (~14) molecules in single crystals have been reported to date using conventional methods and they are all characterized by relatively long lived $\pi$-$\pi^*$ triplet states.

The next major change in the existing paradigm occurred in 1965 when Geschwind, Devlin, Cohen and Chinn[14] reported the optical detection of the ESR of the excited metastable $\bar{E}(2E)$ state of $Cr^{+3}$ in $Al_2O_3$. In this classic experiment they showed that the optical rf double resonance techniques first suggested by Brossel and Kastler[15] and widely used in gases[16] could also be applied to solids. The experiment was performed using a high resolution optical spectrometer to monitor the change in intensity of one of the Zeeman components of the phosphorescence $[\bar{E}(^1E) \rightarrow {}^4A_2]$ as $\bar{E}$ was saturated with microwaves when the magnetic fields was swept through resonance. The resonance signal was observed by modulating the microwave field and detecting the resultant modulation of the optical emission. Since optical rather than microwave photons are detected, the sensitivity can be increased many orders of magnitude over conventional techniques. As an example, at temperatures below the $\lambda$ point of helium the resonance could be observed directly on an oscilloscope without the need for phase sensitive detection. The success in optically detecting the electron spin resonance of a metastable state led several research groups to attempt to apply the same principles to the optical detection of the ESR of organic molecules in their lowest triplet state.

In 1967 the first successful experiment was reported by Sharnoff for the $\Delta M = 2$ transition of naphthalene.[17] In this experiment a single crystal of biphenyl containing 0.1 mole percent naphthalene was placed in a microwave cavity where it was immersed in liquid helium maintained at 1.8°K. The crystal was irradiated with the appropriately filtered light from a mercury arc lamp and the phosphorescence isolated with a detector consisting of a linear polarizer and a low resolution spectrometer. The microwave field was modulated at 40 Hz and the signal detected by feeding the output of the photomultiplier into a phase sensitive amplifier. In this experiment it was shown that the radiative matrix elements connecting any triplet sublevel with the ground singlet electronic level are functions of the magnetic quantum numbers of that sublevel.

At this point the development of ODMR of the lowest triplet state of organic molecules entered a new phase. Now that this new method was shown to be applicable to these molecules the research centered around improving the basic techniques and using this new tool to gain information on a variety of phenomena associated with the triplet state.

Shortly after Sharnoff's paper, Kwiram[18] reported the optical detection of the $\Delta M = 1$ and $\Delta M = 2$ transitions of phenanthrene in its triplet state. In this investigation the experimental methods were the same as those used by Sharnoff except that the microwave field was not modulated while the exciting and emitted light was chopped antisynchronously at 50 Hz. The 50 Hz output of the photomultiplier was converted

to DC by a phase sensitive detector and fed into a signal averager. The observed change in intensity of the phosphorescence at the three transition frequencies was used to assign the spatial symmetry of the triplet state.

Schmidt, Hesselmann, De Groot and van der Waals[19] also reported the optical detection of quinoxaline ($d_6$) in 1967. Their experimental procedure was bascially the same as that used by Sharnoff, except that they modulated the magnetic field with and without amplitude modulation of the microwave field. They were able to show (1) that the emission originates from the top spin component (out-of-plane), and (2) from phosphorescence decay studies, that entry into the triplet state by intersystem crossing is also to the top spin component.

In 1968 Schmidt and van der Waals[20] extended the almost zero field work (3G) of Hutchison's group[21] by optically detecting the zero-field transitions of molecules in their triplet state at zero external magnetic field. Since it is necessary to vary the microwave frequency in order to observe the resonance in zero external magnetic field, a helix was used to couple the microwave power to the sample. The observed signals were extremely sharp and in the case of quinoxaline ($d_6$), showed fine structure.[22]

Tinti, El-Sayed, Maki and Harris[23] extended the method of optical detection in zero field by incorporating a high resolution spectrometer and studying the effect of the microwave field on the individual lines of the phosphorescence spectrum of 2,3-dichloroquinoxaline. This method has since been called Phosphorescence Microwave Double Resonance (PMDR) spectroscopy. They showed that the use of a high resolution spectrometer will give better sensitivity in cases where there is mixed polarization of the phosphorescence, since if the total emission is monitored, the change in intensity due to the microwave field may be partially cancelled. The sensitivity was excellent, and in fact, a very strong signal was observed using C. W. conditions for both the microwave and optical radiations. The observed structure of the zerofield transitions was explained quantitatively in terms of nuclear quadrupole interactions in the excited triplet state in a later paper[24] by Harris et al. and by van der Waals and coworkers [22] in which optically detected electron nuclear double resonance (ENDOR) was reported. Several other papers followed on the observation and interpretation of nitrogen ENDOR in zero field[25-27] and was extended to $^{35}Cl$ and $^{37}Cl$ by Buckley and Harris.[28,29] Optical detection of electron-electron double resonance (EEDOR) was reported by Kuan, Tinti and El-Sayed[30] and was demonstrated to be a method of improving the signal strength of weak zerofield transitions if emission is from only one of the triplet sublevels.

Apart from the applications directly associated with magnetic resonance parameters, ODMR techniques have been used to analyze the phosphorescence spectra. Phosphorescence Microwave Double Resonance (PMDR) spectroscopy technique has already proven itself to be extremely valuable in many applications such as determining the symmetry of the excited state, the pathways of inter- and intramolecular energy transfer for many molecules[31] and other phenomena. Also, utilizing transient microwave excitation, these techniques have been successfully utilized in studying the coherent interactions of excited triplet states with resonant microwave fields. Theoretical aspects of the problem were first considered by Harris[43] followed by a number of experiments including the coherent modulation of the phosphorescence by microwave radiation,[44] the formation of a spin-echo from an excited triplet state,[45] the optical detection of echoes,[46] spin locking,[47] multiple spin echoes,[48] and adiabatic demagnetization.[49] Other experiments have recently been reported, in which the electron spin transitions are induced by coherent acoustic waves[50] and heat pulses or incoherent acoustic waves[51] instead of by a microwave field. These techniques hold the promise of providing a much more detailed picture of the spin-phonon interaction in the excited state.

One of the most promising applications of ODMR and PMDR is the study of exciton interactions in molecular crystals. Using PMDR, the coherent nature of energy exchange between pairs of molecules as nearest neighbors in an isotopically dilute system has been observed.[52] In addition, the coherent migration of triplet Frenkel excitons in molecular crystals has been observed[53] and the density of states function in the band has been measured.[53]

Recently, even the kinetics and quantum yield for the creation of mobile wavepackets in molecular crystals have been determined using these techniques. The methods have also been extended to ionic solids[54] and there is every reason to believe that the techniques will eventually be extended to surface states, molecules adsorbed on surfaces and semiconductors. In short, the potential uses still remaining to be exploited are many and varied. To date, however, techniques of ODMR and PMDR have developed into several basic areas: (1) the study of the electron distribution of organic molecules in their triplet state by analysis of their zero field, nuclear quadrupole and nuclear-electron hyperfine interactions; (2) investigations into the rates and mechanisms of intramolecular processes such as internal conversion and intersystem crossing; (3) as a tool to investigate the energy levels and dynamics properties of exciton bands in molecular crystals; (4) as a method of observing coherent phenomena in the excited states; and (5) as a method of examining spin-phonon interactions. Details of these areas can be found in the work of Sharnoff, Kwiram, van der Waals, Maki, El-Sayed, Harris and others.

The remainder of this article will deal with *only the first of the above areas, and in particular, the measurement of the nuclear quadrupole coupling constants by analysis of the optically detected ESR and ENDOR spectra.*

## II. General Considerations

### A. Sensitivity considerations in the Optical Detection of ESR

One of the primary advantages of optical detection is the excellent sensitivity of about $10^4$ spins as compared to the sensitivity of about $10^{11}$ spins for conventional ESR. This greatly increased sensitivity permits the detection of the ESR of molecules with very short excited state lifetimes. In this section a cursory analysis of the influence of various properties of the excited state on the sensitivity with optical detection are presented. Although many kinetic schemes can be constructed for various experiments, we consider experiments performed under conditions of continuous optical excitation while monitoring the change in intensity of the phosphorescence as a function of the applied microwave field.[33,55] Only the case in which the triplet state is populated by excitation of the sample into the first excited singlet state followed by intersystem crossing into the triplet state will be considered. For molecules with reasonably high symmetry (i.e., $D_{2h}$, $C_{2h}$, and $C_{2v}$) different modes of populating the triplet state produce to varying degrees a different spin alignment. This is illustrated in Figure 1 where the radiative and nonradiative pathways for energy transfer are depicted. $[S_1]$ is the population of the lowest excited singlet state, $[N_\chi]$ ($\chi = x,y,z$) is the steady state population of the corresponding triplet levels, $K_{1\chi}$ is the intersystem crossing rate constant from $S_1$ to $T_1$, $K_\chi$ is the radiative or phosphorescence rate constant for relaxation to $S_o$, $K_{nx}$ is the non-radiative decay or relaxation rate constant from $T_1$ to $S_o$, $W_{\chi_1\chi_2}(\chi_1 \neq \chi_2)$ is the spin lattice relaxation rate constant and $P_{\chi_1\chi_2}(\chi_1 \neq \chi_2)$ is the induced rate constant due to the applied microwave field ($H_1$). When the microwave field does not connect any two of the zero field levels of the triplet, the steady state population is given by setting $P_{\chi_1\chi_2} = 0$. The application of the microwave field at a frequency corresponding to the energy

separation of two of the levels (i.e., $\nu = (E_x - E_y)/h$) causing a redistribution of the population which in most cases results in a change in the phosphorescence intensity. Since optical, rather than microwave, photons are detected, one expects the sensitivity to be improved in proportion to the ratio of the energies of the photons, which, for a typical molecule, is approximately $3 \times 10^5$. The actual change in the phosphorescence intensity, however, is a complex function of the various relaxation channels and rate constants. The actual improvement in sensitivity depends on the molecule under study.

In order to derive a reasonably simple quantitative expression for the change in intensity of the phosphorescence, the three following assumptions will be made:

1) The splitting of the three triplet zero field levels by nuclear quadrupole and nuclear hyperfine interactions will be neglected,

2) Only the two levels connected by the $H_1$ field will be considered; these are designated $\tau_x$ and $\tau_y$, and

3) Only the steady state condition, $dN_x/dt = dN_y/dt = 0$, will be considered for both the case when $H_1 = 0$ and $H_1 \neq 0$.

The first assumption will predict too great a change in intensity if the individual triplet levels are split by more than the frequency width of the $H_1$ field, since in this case the $H_1$ field will allow an additional relaxation pathway for only a fraction of the population of each triplet level at any given frequency. The second assumption will introduce an error in the expression for the percentage change in intensity

since the intensity contribution from the level not connected by the $H_1$ field ($\tau_z$) is neglected. This assumption also requires that the spin lattice relaxation rate between $\tau_z$ and $\tau_x$ and between $\tau_z$ and $\tau_y$ be neglected. This is usually valid since the experiments are performed at or below 4.2° K. The third assumption requires that the experiment be performed using C. W. microwave conditions or modulating the microwave field with a frequency lower than the total rate constant of the system.

The differential equations describing the population of the levels shown in Figure 2 are

$$\frac{dN_x}{dt} = S_1K_{1x} - N_x [K_{nx} + K_x + W_{xy} + P_{xy}] + N_y [W_{yx} + P_{xy}] \quad (9)$$

$$\frac{dN_y}{dt} = S_1K_{1y} - N_y [K_{ny} + K_y + W_{yx} + P_{xy}] + N_x [W_{xy} + P_{xy}] \quad (10)$$

With the definitions

$$\begin{aligned} A &= K_{nx} + K_x + W_{xy} + P_{xy} \\ B &= W_{yx} + P_{xy} \\ C &= K_{ny} + K_y + W_{yx} + P_{xy} \\ D &= W_{xy} + P_{xy} \end{aligned} \quad (11)$$

Equations 9 and 10 may be rewritten

$$\frac{dN_x}{dt} = S_1K_{1x} - N_xA + N_yB \quad (12)$$

$$\frac{dN_y}{dt} = S_1K_{1y} - N_yC + N_xD \tag{12}$$

The steady state assumption allows us to write

$$\frac{dN_x}{dt} = S_1K_{1x} - N_xA + N_yB = 0 \tag{14}$$

$$\frac{dN_y}{dt} = S_1K_{1y} - N_yC + N_xD = 0 \tag{15}$$

Upon solving Equations 14 and 15 for the population of the triplet levels, we have

$$N_x = \frac{S_1[CK_{1x} + BK_{1y}]}{AC - BD} \tag{16}$$

and

$$N_y = \frac{S_1[AK_{1y} + DK_{1x}]}{AC - BD} \tag{17}$$

The intensity of the phosphorescence detected with an optical spectrometer may be written

$$I = \alpha_1N_xK_x + \alpha_2N_yK_y \tag{18}$$

where $\alpha_1$ and $\alpha_2$ are constants that depend on the polarization of the emission, the orientation of the sample, and the efficiency of the detection system. The assumption will be made that $\alpha_1 = \alpha_2$, which allows the fractional change in the intensity of the phosphorescence upon application of the $H_1$ field to be written

$$\Delta I = \frac{I - I_o}{I_o} = \frac{I}{I_o} - 1 \tag{19}$$

where $I_o$ is the intensity of the phosphorescence when $P_{xy} = 0$. With this condition, it is convenient to define the parameters given in Equation 11 as

$$\begin{aligned} a &= K_{nx} + K_x + W_{xy} \\ b &= W_{yx} \\ c &= K_{ny} + K_y + W_{yx} \\ d &= W_{xy} \end{aligned} \tag{20}$$

If both of the triplet levels are monitored, the fractional change in intensity of the emission is given by

$$\Delta I = \left\{ \frac{[K_{1y}(AK_y + BK_x) + K_{1x}(CK_x + DK_y)][ac - bd]}{[K_{1y}(aK_y + bK_x) + K_{1x}(cK_x + dK_y)][AC - BD]} \right\} - 1 \tag{21}$$

In some cases it is possible to monitor only one of the triplet levels connected by the $H_1$ field, in which case the change in intensity of emission from the $\tau_x$ and $\tau_y$ levels are given by

$$\Delta I_x = \left\{ \frac{[CK_{1x} + BK_{1y}][ac - bd]}{[cK_{1x} + bK_{1y}][AC - BD]} \right\} - 1 \tag{22}$$

and

$$\Delta I_y = \left\{ \frac{[AK_{1y} + DK_{1x}][ac - bd]}{[aK_{1y} + dK_{1x}][AC - BD]} \right\} - 1 \tag{23}$$

Three cases will be discussed in order to examine the effect of the magnitude of the various rate constants on the sensitivity of the experiment.

Case #1, The Effect of Radiative Decay

For illustration purposes, we assume that the non-radiative and spin lattice relaxation rate constants may be neglected. The parameters defined in Equations 11 and 20 become

$$\begin{aligned} A &= K_x + P_{xy} & a &= K_x \\ B &= P_{xy} & b &= 0 \\ C &= K_y + P_{xy} & c &= K_y \\ D &= P_{xy} & d &= 0 \end{aligned} \tag{24}$$

In the absence of the $H_1$ field the steady state populations are given by

$$\begin{aligned} N_x^o &= S_1(K_{1x}/K_x) \\ N_y^o &= S_1(K_{1y}/K_y) \end{aligned} \tag{25}$$

The steady state population of $\tau_x$ is given by Equation 16 which for this example becomes

$$N_x = \frac{S_1[K_{1x}K_y + P_{xy}(K_{1x} + K_{1y})]}{[K_xK_y + P_{xy}(K_x + K_y)]} \tag{26}$$

In the limit that $P_{xy}$ is much larger than any of the relaxation rate constants, the populations of $\tau_x$ and $\tau_y$ are equalized and the transition is saturated. Clearly, the power required to equalize the populations is directly proportional to the relaxation rate of the

system and inversely proportional to the lifetime of the excited state. The population of $\tau_x$ at saturation is given by

$$N_x^s = \frac{S_1[K_{1x} + K_{1y}]}{[K_x + K_y]} \tag{27}$$

and the corresponding population of $\tau_y$ is given by

$$N_y^s = \frac{S_1[K_{1x} + K_{1y}]}{[K_x + K_y]} \tag{28}$$

and therefore, $N_x^s = N_y^s$. The change in population of $\tau_x$ upon saturation is

$$\Delta N_x = N_x^s - N_x^o = \frac{S_1[K_xK_{1y} - K_yK_{1x}]}{K_x(K_x + K_y)} \tag{29}$$

Therefore, if $K_xK_{1y} = K_yK_{1x}$, there is no change in population. If the emissions from $\tau_x$ and $\tau_y$ are monitored simultaneously, the fractional change in intensity is given by Equation 21 which, for this example, reduces to

$$\Delta I = \left\{\frac{[K_{1y}(AK_y + BK_x) + K_{1x}(CK_x + DK_y)]}{[K_{1y}(AC - BD)]}\right\} - 1 \tag{30}$$

$$= \left\{\frac{[K_{1x} + K_{1y}][P_{xy}(K_x + K_y) + K_xK_y]}{[K_{1x} + K_{1y}][P_{xy}(K_x + K_y) + K_xK_y]}\right\} - 1 \tag{31}$$

In such a case, $\Delta I = 0$ and no change in the intensity of emission will be observed. However, if a high resolution optical spectrometer is

used, it is often possible to monitor the emission from just one of the triplet levels via its selective emission to the origin or a vibration of the ground state singlet manifold. Consider for example, emission from $\tau_x$, which case the change in intensity given by Equation 22 becomes

$$\Delta I_x = \frac{K_x}{K_{lx}}\left[\frac{P_{xy}(K_{lx} + K_{ly}) + K_{lx}K_y}{P_{xy}(K_x + K_y) + K_xK_y}\right] - 1 \qquad (32)$$

In the limiting case where intersystem crossing proceeds primarily to $\tau_x$ $(K_{lx} \gg K_{ly})$ Equation 32 reduces to

$$\Delta I_x = \left|\frac{P_{xy}K_x + K_xK_y}{P_{xy}(K_x + K_y) + K_xK_y}\right| - 1 \qquad (33)$$

At saturation we have

$$\Delta I_x^s = \left(\frac{K_x}{K_x + K_y}\right) - 1 \qquad (34)$$

The effect of the ratio of the radiative rate constants $(K_x/K_y)$ on the maximum change in intensity of the emission may be illustrated with the following examples:

| $K_x/K_y$ | $\Delta I_x^s$ (%) |
|---|---|
| 0.1 | 91 |
| 1 | 50 |
| 10 | 9 |

It is apparent than the maximum sensitivity is achieved if the level with the fast intersystem crossing rate constant has the slower phosphorescence rate constant.

Case #2, The Effect of Spin Lattice Relaxation

The two rate constants for spin lattice relaxation are not independent and may be related directly to the spin lattice relaxation time $T_1$ for any given temperature.

The interaction between the energy and the lattice may be represented schematically as

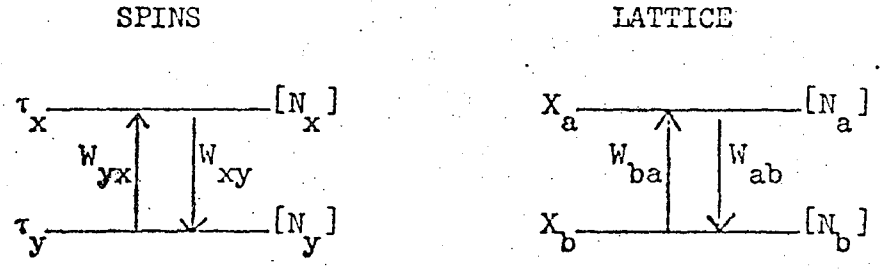


The conservation of energy requires that for each transition from $\tau_x$ to $\tau_y$ there be a corresponding lattice transition from $X_b$ to $X_a$ and vice versa. The transition rate for the lattice is written

$$W_{ab} = N_a A$$
$$W_{ba} = N_b A \qquad (35)$$

where $A$ is the transition probability. The spin lattice relaxation rate constants may be written in terms of the population of the lattice as

$$W_{xy} = W_{ba} = N_b A$$
$$W_{yz} = W_{ab} = N_a A \qquad (36)$$

Since the lattice is at the temperature of the bath (liquid helium), the normalized population of the lattice is given by

$$N_a = \frac{e^{-\delta/2kt}}{e^{-\delta/2kt} + e^{\delta/2kt}} = f$$
$$N_b = \frac{e^{\delta/2kt}}{e^{-\delta/2kt} + e^{\delta/2kt}} = 1 - f \qquad (37)$$

where $\delta = (E_x - E_y)$ and $E_x$ and $E_y$ are the energies of the x and y magnetic sublevels respectively. The spin lattice relaxation rates may now be written

$$W_{xy} = (1 - f)\, A$$
$$W_{yx} = (f)\, A \qquad (38)$$

The spin lattice relaxation time is defined by the expression

$$T_1 = \frac{1}{W_{xy} + W_{yx}} = \frac{1}{A} \qquad (39)$$

and $W_{xy}$ and $W_{yx}$ may be expressed in terms of $T_1$ and f as

$$W_{xy} = \frac{1 - f}{T_1}$$
$$W_{yx} = \frac{f}{T_1} \qquad (40)$$

In the derivation of Equation 40 it is assumed that only a direct process of energy transfer between the spin system and the lattice exists which is usually the case at the temperatures of the experiments (4.2° to 1.3°K). If Raman or Orbach processes are present, only the explicit temperature dependence of the relaxation must be corrected so that the spin lattice relaxation may always be defined for a two level system in terms of only $T_1$ at a given temperature. A short $T_1$ relaxation time will tend to produce a Boltzmann population distribution between the spin sublevels and will significantly reduce the spin alignment. This can be seen by considering the simple case where there is only intersystem crossing to $\tau_x$ and emission from $\tau_x$ and $\tau_y$. Again the non-radiative decay rate constants $K_{nx}$ and $K_{ny}$ are assumed to be negligible. The parameters defining this model are

$$\begin{aligned} A &= K_x + W_{xy} + P_{xy} & a &= K_x + W_{xy} \\ B &= W_{yx} + P_{xy} & b &= W_{yx} \\ C &= K_y + W_{yx} + P_{xy} & c &= K_y + W_{yx} \\ D &= W_{xy} + P_{xy} & d &= W_{xy} \end{aligned} \tag{41}$$

and the populations of $\tau_x$ and $\tau_y$ when $P_{xy} = 0$ are given by

$$N_x^o = \frac{S_1[(K_y + W_{yx})K_{lx}]}{K_xK_y + K_yW_{xy} + K_xW_{yx}} \tag{42}$$

and

$$N_y^o = \frac{S_1[(W_{xy})K_{lx}]}{K_xK_y + K_yW_{xy} + K_xW_{yx}}$$

In the limit that $W_{xy} = W_{yx} = 0$ this reduces to

$$N_x^o = \frac{S_1[K_{1x}]}{K_x}$$
$$N_y^o = 0 \qquad (43)$$

At high temperatures when $W_{xy} \approx W_{yx} \gg K_x, K_y, K_{1x}$, Equation 42 becomes

$$N_x^o = \frac{S_1[K_{1x}]}{K_x + K_y}$$
$$N_y^o = \frac{S_1[K_{1x}]}{K_x + K_y} \qquad (44)$$

Since the change in population is monitored, it is clearly advantageous to perform the experiments at the lowest possible temperature in order to decrease the thermalization of the spin levels and the resulting loss in sensitivity.

Case #3, The Effect of Non-Radiative Relaxation

The final case to be considered is the effect of the non-radiative relaxation rate constants $K_{nx}$ and $K_{ny}$ on the sensitivity of the experiment. It is obvious that since only the radiative emission is detected, a large rate of depopulation by non-radiative relaxation is not desirable, unless it produces enhanced spin alignment. In the case of a sample that relaxes primarily through nonradiative pathways, the sensitivity may be improved by ising conventional ESR techniques and monitoring the absorption of microwave

power, or in extreme cases by monitoring the change in temperature of the sample. A quantitative measure of the decrease in sensitivity may be calculated by substituting the appropriate rate constants into Equations 21, 22 and 23; however, the expressions are rather complex and therefore not particularly useful.

It should be noted that although we have dealt with the rate processes in the discussion of sensitivity, the results can be used to measure the relative rate processes associated with the individual magnetic sublevels. Specifically, the measurement of intensity changes of phosphorescence under the influence of the microwave field can yield the relative intersystem crossing, radiative and radiationless rate constants to and from all three magnetic sublevels. Indeed, this approach has already been widely applied [56] in the limit that spin-lattice relaxation may be neglected and saturation of the transition is achived. The inclusion of the power factor, however, gives one an additional experimental "handle" from which to extract information (cf. Equations 21, 22 and 23).

B. Optically Detected ENDOR

The sensitivity of this experiment may be estimated if the assumption is made that there is no nuclear polarization. Since this assumption has yet to be thoroughly investigated, it is reasonable to expect that in some cases it will not be valid. Nuclear polarization may arise through cross relaxation between the electron and nuclear spin systems (the Overhauser effect), or it may be induced by saturation

of "forbidden" transitions (simultaneous electron-nuclear flips). It is also possible that selective intersystem crossing may preferentially populate a particular nuclear spin level if there is strong hyperfine coupling of the electron and nuclear wavefunctions.

In the absence of nuclear polarization, the sensitivity of the optically detected ENDOR signal may be understood by referring to Figure 3 in which the $\tau_x$ and $\tau_y$ triplet levels are now each composed of two levels. This splitting of the triplet levels is due to nuclear quadrupole and hyperfine interactions as will be discussed in the following sections. The results obtained by considering the triplet levels as being split into only two nuclear sublevels are independent of the number of sublevels if the ESR transition connects only one nuclear sublevel in each of the two triplet levels, and the ENDOR transition connects only two nuclear sublevels in one of the triplet levels.

As has already been discussed, the sensitivity of the optical detection technique is dependent on the various relaxation pathways from the triplet state. The same considerations apply in an ENDOR experiment. Since the sensitivity of the ENDOR experiment will be referenced to the sensitivity of the ESR experiment, the explicit dependence of the triplet state populations on the various rate constants need not be specified. For the system shown in Figure 3, the phosphorescence intensity may then be written

$$I_o = 2(N_x K_x + N_y K_y) \tag{45}$$

where $N_x$ ($N_y$) is now defined as the population of each of the two levels in the $\tau_x$ ($\tau_y$) manifold.

Upon saturation of the electron spin transition $(b \leftrightarrow d)$, this becomes

$$I_S = \left(\frac{3N_x + N_y}{2}\right)K_x + \left(\frac{3N_y + N_x}{2}\right)K_y \tag{46}$$

with the change in intensity given by

$$\Delta I = I_S - I_o = \tfrac{1}{2}(N_x - N_y)(K_y - K_x) \quad . \tag{47}$$

If the ENDOR transition $(a \leftrightarrow b)$ is also saturated, the intensity is given by

$$I_E = \frac{2}{3}\left[(2N_x + N_y)K_x + (2N_y + N_x)K_y\right] \quad . \tag{48}$$

Since the ENDOR signal is detected by monitoring the change in intensity of the ESR transition, the signal strength is given by

$$\Delta I_E = I_E - I_S \tag{49}$$

$$= \frac{1}{6}\left[(N_x - N_y)(K_y - K_x)\right] \tag{50}$$

and the fractional change in intensity of the ESR signal upon saturation of the ENDOR transition is

$$\delta I = \Delta I_E / \Delta I_S = \frac{1}{3} \quad . \tag{51}$$

If the ENDOR transition $(c \leftrightarrow d)$ is saturated instead of the transition from $(a \leftrightarrow b)$, the same expression is obtained for the change in intensity (Equations 50 and 51).

It is interesting to note from Equations 47 and 50 that the ESR signal and the ENDOR signal always affect the intensity of the phosphorescence in the same direction.

If the forbidden ESR transition from $(b \leftrightarrow c)$ is saturated and if the two ENDOR transitions $(a \leftrightarrow b)$ and $(c \leftrightarrow d)$ occur at the same frequency, the change in phosphorescence intensity is given by

$$\Delta I_E = \frac{1}{2}[(N_x - N_y)(K_y - K_x)] \tag{52}$$

and the fractional change in intensity of the ESR signal is unity.

As a final note, if the ESR transitions from $(a \leftrightarrow c)$ and $(b \leftrightarrow d)$ occur at the same frequency, the ENDOR transitions from $(a \leftrightarrow b)$ and $(c \leftrightarrow d)$ must also occur at the same frequency causing the change in intensity of the ESR signal to be twice as large (Equation 47),

$$\Delta I = (N_x - N_y)(K_y - K_x) \tag{53}$$

while the ENDOR transitions will not be observed since the populations of the nuclear sublevels are already equal.

## III. The Zero Field Spin Hamiltonian

The observed magnetic resonance spectra of the excited triplet state of organic molecules in zero external magnetic field may be understood in terms of a Hamiltonian of the form,

$$H = H_{SS} + H_Q + H_{HF}$$

where $H_{SS}$ is the spin-spin or zero field interaction between the two unpaired electrons, $H_Q$ is the nuclear quadrupole interaction, and $H_{HF}$ is the nuclear electron hyperfine interaction.

A. $H_{SS}$ -- The Spin-spin or Zero Field Splitting Hamiltonian

$H_{SS}$ is primarily due to the magnetic dipole-dipole interaction between the unpaired electrons in the excited triplet state. There can also be a contribution from the spin orbit coupling between the lowest triplet and other excited states; however, the contribution from the interaction between other excited triplet states of the same orbital type shifts the three levels equally,[57] and for our purposes will be neglected.

If the radiative lifetime for fluorescence and phosphorescence is known, the magnitude of the spin-orbit contribution to the zero field splitting may be estimated by choosing a simple model in which the transition probability for phosphorescence is due only to the spin-orbit coupling of one spin sublevel with only one excited singlet state. In the framework of this model the transition probability for phosphorescence may be expressed as

$$P_p \approx |\langle {}^3\psi_1| \, e\vec{r} \, |{}^1\psi_o\rangle|^2 = \frac{1}{\tau_p} \qquad (54)$$

where $e\vec{r}$ is the electron dipole moment transition operator, ${}^3\psi_1$ is the first triplet state, ${}^1\psi_o$ is the ground singlet state, and $\tau_p$ is the phosphorescence radiative lifetime. The wave function for the phosphorescent triplet state is actually a linear combination of the pure triplet state, which is spin forbidden for electric dipole radiation to

the ground state, and an admixture of singlet character due to spin-orbit coupling. $^3\psi_1$ may be represented as a linear combination of $^3\psi_1^o$ and $^1\psi_1^o$ as

$$^3\psi_1 = C_1\, ^3\psi_1^o + C_2\, ^1\psi_1^o \tag{55}$$

where $^3\psi_1^o$ and $^1\psi_1^o$ are the wave functions for the first excited singlet and triplet states respectively in the absence of spin-orbit coupling. In organic molecules the spin orbit matrix element is generally small so $C_1 \approx 1$ and $C_2$ is given from perturbation theory as

$$C_2 = \frac{\langle ^1\psi_1^o |\ H_{SO}\ | ^3\psi_1^o \rangle}{|^1E_1 - {}^3E_1|} = \frac{\delta}{|^1E_1 - {}^3E_1|} \quad . \tag{56}$$

where $^1E_1$ is the energy of $^1\psi_1$ and $^3E_1$ is the energy of $^3\psi_1$. The phosphorescence transition probability (Equation 54) is simply

$$\frac{1}{\tau_P} = |\langle C_1\, ^3\psi_1^o + C_2\, ^1\psi_1^o |\ e\vec{r}\ |\, ^1\psi_o \rangle|^2 \tag{57}$$

$$= C_2^2\, |\langle ^1\psi_1^o |\ e\vec{r}\ |\, ^1\psi_o \rangle|^2$$

while the fluorescence transition probability is given by

$$P_F \approx |\langle ^1\psi_1 |\ e\vec{r}\ |\, ^1\psi_o \rangle|^2 = \frac{1}{\tau_F} \quad . \tag{58}$$

Substituting Equation 58 into Equation 57, we have

$$C_2^2 = \frac{\tau_F}{\tau_P} = \frac{\delta^2}{|^1E_1 - {}^3E_1|^2} \tag{59}$$

Within the limits of the model, the spin-orbit matrix element is given by

$$\delta = \left(\frac{\tau_F}{\tau_P}\right)^{\frac{1}{2}}\left({}^1E_1 - {}^3E_1\right) \tag{60}$$

Also from perturbation theory the shift in energy of the triplet zero field level coupled to ${}^1\psi_1$ may be written

$$\Delta = \frac{\delta^2}{|{}^1E_1 - {}^3E_1|} = \left(\frac{\tau_F}{\tau_P}\right)\left({}^1E_1 - {}^3E_1\right) \tag{61}$$

As an example, for benzene,[58] $\tau_P = 30$ sec, $\tau_F = 3 \times 10^{-8}$ sec, and assuming $|{}^1E_1 - {}^3E_1| \leq 6000$ cm$^{-1}$, we have,

$$\Delta = \frac{3 \times 10^{-8} \text{ sec}}{30 \text{ sec}} \quad (6000 \text{ cm}^{-1})$$

$$= 6 \times 10^{-5} \text{cm}^{-1}$$

Compared to the measured zero field splittings of benzene[59] of 0.1644 cm$^{-1}$, 0.1516 cm$^{-1}$, and 0.0128 cm$^{-1}$, the spin-orbit coupling contribution to the zero field splitting is clearly negligible.

An example of the magnitude of the effect is given by paradichlorobenzene[60] for which $\tau_P = 16$ ms., $\tau_F = 3 \times 10^{-8}$ sec, and $|{}^1E_1 - {}^3E_1| \leq 7800$ cm$^{-1}$. Substituting these values into Equation 61, we find that $\Delta = 1.5 \times 10^{-2}$ cm$^{-1}$. This is still small compared to the observed zero field splittings[29] of 0.1787 cm$^{-1}$, 0.1201 cm$^{-1}$, and 0.0584 cm$^{-1}$. In addition, since we used

the measured lifetime of the phosphorescence which includes both the radiative and non-radiative transition probabilities, the actual contribution of spin-orbit coupling to the zero field splitting is certainly smaller. For organic molecules in their excited triplet state, the splitting of the zero field levels due to spin-orbit coupling usually accounts for only a small percentage of the observed zero field splitting and therefore, we will consider on the magnetic dipole-dipole interaction in explaining the observed spectra. The addition of a heavy atom however will increase the spin orbit coupling matrix element.

The Hamiltonian for magnetic dipole-dipole interaction between two unpaired electrons may be written[61] as

$$H_{SS} = g_e^2 \beta_e^2 \left\{ \frac{S_1 \cdot S_2}{r^3} - \frac{3(S_1 \cdot r)(S_2 \cdot r)}{r^5} \right\} \qquad (62)$$

where $g_e$ is the electron g factor, which has been found to be basically isotropic for aromatic triplet states and equal to the free electron value of 2.00232, $\beta_e$ is the Bohr magneton ($eh/2mc$), and $r$ is the vector connecting the two electron spins $S_1$ and $S_2$. The Hamiltonian is of the same form as any dipole-dipole interaction, and in the case of the interaction between the two triplet state electrons is expressed as

$$H_{SS} = S \cdot D \cdot S \qquad (63)$$

which may be written in a Cartesian axis system as

$$H_{SS} = D_{xx}S_x^2 + D_{xy}S_xS_y + D_{xz}S_xS_z + D_{yx}S_yS_x + D_{yy}S_y^2 + D_{yz}S_yS_z + D_{zx}S_zS_x + D_{zy}S_zS_y + D_{zz}S_z^2 \quad (64)$$

The values of the $D_{ij}$ $(i,j = x,y,z)$ are given by averages over the triplet state electronic wave function[62]

$$D_{xx} = \frac{1}{2} g_e^2\beta^2\left\langle\frac{r^2 - 3x^2}{r^5}\right\rangle$$
$$D_{xy} = \frac{1}{2} g_e^2\beta^2\left\langle\frac{-3xy}{r^5}\right\rangle \quad (65)$$

and so on. D is a symmetrical tensor ($D_{xy} = D_{yx}$, etc.); therefore, in the principal axis system which diagonalizes the zero field tensor, the Hamiltonian becomes

$$H_{SS} = -XS_x^2 - YS_y^2 - ZS_z^2 \quad (66)$$

where $X = -D_{xx}$, $Y = -D_{yy}$, and $Z = -D_{zz}$

Since the Hamiltonian is traceless, $X + Y + Z = 0$, only two independent parameters are needed to describe the interaction. In conventional ESR the Hamiltonian in the principal axis system is usually rewritten by defining

$$D = \frac{1}{2}(X + Y) - Z \quad \text{and} \quad E = -\frac{1}{2}(X - Y) \quad (67)$$

with the axis convention that $|X| \leq |Y| \leq |Z|$. Therefore, the three components of the Hamiltonian are given by

$$X = D/3 - E$$
$$Y = D/3 + E \qquad (68)$$
$$Z = -2/3\ D$$

Thus, for the triplet state, the zero field spin-spin interaction can be written in diagonal form as

$$H_{SS} = D(S_z^2 - 2/3) + E(S_x^2 - S_y^2) \qquad (69)$$

where the triplet electron representations X, Y, and Z are related to the $S_z$ eigenstates by:

$$|X> = 1/\sqrt{2}\ (|-1> - |1>)$$
$$|Y> = i/\sqrt{2}\ (|-1> + |1>) \qquad (70)$$
$$|Z> = |0>$$

This form of the Hamiltonian is directly related to the chosen axis system of the molecule and presents a clear picture of the orientational dependence of the energy.

The usual selection rule in ESR of $\Delta S_z = \pm 1$ is not valid in zero magnetic field since the triplet sublevels are not eigenfunctions of $S_z$. The probability of magnetic dipole transitions between the triplet spin sublevels are given by

$$P_{x\to y} = |<X|\ S_z\ |Y>|^2 = 1$$
$$P_{x\to z} = |<X|\ S_y\ |Z>|^2 = 1 \qquad (71)$$
$$P_{y\to z} = |<Y|\ S_x\ |Z>|^2 = 1$$

At this time we should point out an obvious feature about the form of the electron spin dipolar Hamiltonian. *It is identical in form to the nuclear quadrupole Hamiltonian.* In fact, the zerofield electron spin Hamiltonian for triplet spins is identical to the $^{14}N$ nuclear quadrupole Hamiltonian save for the replacement of $I^2$ operators for $S^2$ operators. This means that nuclear quadrupole interactions in excited states will appear in zeroth order as satellite transitions split off the zerofield electron spin transition by the appropriate quadrupole interaction energy. As we shall see, however, these satellite transitions are shifted slightly by first order nuclear electron hyperfine interactions.

B. $H_Q$ -- The Nuclear Quadrupole Hamiltonian

As is wellknown, nuclei with spins ≥ 1 have non-spherical charge distribution and therefore an electric quadrupole moment. The quadrupole moment of the nucleus is positive or negative depending on whether the charge distribution is elongated or flattened along the spin axis and each allowed nuclear orientation along the spin axis has associated with it a potential energy due to the surrounding electric field. In the case of a molecule, the electric field is due to non-s electrons which produce a field gradient ($V_{i,j}$) at the nucleus defined by

$$V_{i,j} = \frac{\partial^2 V}{\partial_i, \partial_j} \quad (i,j = x,y,z) \tag{72}$$

where V is the electrostatic potential at the nucleus.

In an arbitrary axis system the Hamiltonian[63] is written as

$$\begin{aligned} H_Q = B \Big\{ & V_{zz}(3I_z^2 - I^2) + (V_{zx} + i\,V_{zy})(I_-I_z + I_zI_-) \\ & + (V_{zx} - i\,V_{zy})(I_+I_z + I_zI_+) + [1/2(V_{xx} - V_{yy}) \\ & + i\,V_{xy}]\,I_+^2 + [1/2(V_{xx} - V_{yy}) - i\,V_{xy}]\,I_-^2 \Big\} \end{aligned} \tag{73}$$

where $B = \frac{eQ}{4I(2I-1)}$

$e$ = the electron charge (esu)

$Q$ = the quadrupole moment ($cm^2$)

and $I$ = the nuclear spin quantum number.

The Hamiltonian being a symmetric tensor and like the electron spin dipolar Hamiltonian can be transformed to an axis system such that $V_{i,j} = 0$ for $i \neq j$, where the Hamiltonian is rewritten as:

$$H_Q = B\left\{V_{zz}(3I_z^2 - I^2) + [1/2(V_{xx} - V_{yy})(I_+^2 + I_-^2)]\right\} . \quad (74)$$

Because the Laplace equation is satisfied:

$$V_{xx} + V_{yy} + V_{zz} = 0 . \quad (75)$$

and consequently, only two independent parameters are used to describe the interaction. The conventional nomenclature in nuclear quadrupole resonance spectroscopy defines the field gradient, q, and the asymmetry parameter, $\eta$, by the relations

$$eq = V_{zz}$$
$$\eta = \frac{V_{xx} - V_{yy}}{V_{zz}} . \quad (76)$$

with the convention

$$|V_{xx}| \leq |V_{yy}| \leq |V_{zz}| \quad (77)$$

The standard form of the Hamiltonian, Equation 74, is rewritten as

$$H_Q = A\left[(3I_z^2 - I^2) + \eta/2\,(I_+^2 + I_-^2)\right] \quad (78)$$

where $A = \frac{e^2qQ}{4I(2I-1)}$ .

This may also be written in the completely equivalent form

$$H_Q = A\,[(3I_z^2 - I^2) + \eta(I_x^2 - I_y^2)] \tag{79}$$

One should note the similarity of Equation 79 to Equation 69. The Hamiltonian matrix consists of diagonal terms and off-diagonal terms connecting states differing in $I_z$ by $\pm 2$. The electric potential due to the relative orientation of $H_Q$ to $H_{ss}$ can effect the "apparent" magnitude of $H_Q$ since $H_Q$ manifests itself as a perturbation on $H_{ss}$.

Because we will explicitly deal with $^{35}Cl$ and $^{14}N$ quadrupole interactions in excited states, we *review* the explicit form of the Hamiltonian for I = 1 and I = 3/2.

The Hamiltonian for an I = 1 nucleus ($^{14}N$) is expressed in a more convenient form by transforming Equation 79 to the representation in which the energy is diagonal. In this representation, the Hamiltonian is in the same form as the electron spin-spin Hamiltonian, and is particularly convenient since it may be written in terms of the nuclear angular momentum operators as

$$H_Q = -xI_x^2 - yI_y^2 - zI_z^2 \tag{80}$$

For a spin of I = 3/2 it is easier to use matrix notation, i.e.

$$H_Q = \frac{e^2qQ}{4} \cdot \tag{81}$$

| | $\lvert 3/2\rangle$ | $\lvert 1/2\rangle$ | $\lvert -1/2\rangle$ | $\lvert -3/2\rangle$ |
|---|---|---|---|---|
| | 1 | 0 | $\eta/\sqrt{3}$ | 0 |
| | 0 | -1 | 0 | $\eta/\sqrt{3}$ |
| | $\eta/\sqrt{3}$ | 0 | -1 | 0 |
| | 0 | $\eta/\sqrt{3}$ | 0 | 1 |

The matrix may be rewritten as two separate 2 x 2 matrices by re-arranging the order of the basis states as

$$H_Q = \frac{e^2qQ}{4} \cdot \begin{array}{c|cccc} & |3/2> & |-1/2> & |1/2> & |-3/2> \\ \hline |3/2> & 1 & \eta/\sqrt{3} & 0 & 0 \\ |-1/2> & \eta/\sqrt{3} & -1 & 0 & 0 \\ |1/2> & 0 & 0 & -1 & \eta/\sqrt{3} \\ |-3/2> & 0 & 0 & \eta/\sqrt{3} & 1 \end{array} \qquad (82)$$

The eigenvalues of the Hamiltonian are simply obtained by diagonalizing each of the 2 x 2 matrices.

$$E_{\pm 3/2} = \frac{e^2qQ}{4}\left(1 + \eta/3\right)^{1/2}$$
$$E_{\pm 1/2} = \frac{-e^2qQ}{4}\left(1 + \eta/3\right)^{1/2} \qquad (83)$$

The eigenstates are

$$|3/2>' = a|3/2> + b|-1/2>$$
$$|-1/2>' = a|-1/2> - b|3/2>$$
$$|1/2>' = a|1/2> - b|-3/2> \qquad (84)$$
$$|-3/2>' = a|-3/2> + b|1/2>$$

where

$$a = \frac{1 + \sqrt{1 + x^2}}{[2(1 + x^2 + \sqrt{1 + x^2})]^{1/2}} \qquad (85)$$

$$b = x/\left[2(1 + x^2 + \sqrt{1 + x^2})\right]^{1/2}$$

and $$x = \eta/3$$

In contrast to a nucleus with spin $I = 1$, $e^2qQ$ and $\eta$ cannot be determined. It should be noted, however, that the transition frequency is not particularly sensitive to $\eta$. The assumption that $\eta = 0$ and the transition energy is equal to $(1/2)e^2qQ$ will produce only a small error for small values of $\eta$.

C. $H_{HF}$ -- The Nuclear Electron Hyperfine Interaction

A nucleus with a spin $\geq 1/2$, like an electron, has a magnetic moment and the interaction of this nuclear magnetic moment with the electron magnetic moment leads to both an anisotropic dipole-dipole interaction and a Fermi contact interaction due to a finite electron spin density at the nucleus.

The component of the hyperfine interaction, due to the interaction of the nuclear and electron magnetic moments, is entirely analogous to the zero field Hamiltonian with the replacement of one of the electron

spins with a nuclear spin and the appropriate change of constants. The Hamiltonian[62] may be written as

$$H_{HF}^{DD} = - g_e \beta_e g_n \beta_n \left[ \frac{I \cdot S}{r^3} - \frac{3(I \cdot r)(S \cdot r)}{r^5} \right] \quad (86)$$

and $g_n$ is the nuclear g factor and $\beta_n$ is the nuclear magneton. Since this is identical in form to Equation 62 for the zero field Hamiltonian, Equation 86 is expressed as

$$H_{HF}^{DD} = S \cdot A \cdot I \quad (87)$$

which can be expanded in the same manner as Equation 64. The A matrix is symmetric and therefore, in its principal axis system, it is written as

$$H_{HF}^{DD} = A_{xx} S_x I_x + A_{yy} S_y I_y + A_{zz} S_z I_z \quad (88)$$

where the hyperfine elements are given by the average over the spatial distribution of the unpaired spins

$$A_{\chi\chi} = - g_e g_n \beta_e \beta_n \left\langle \frac{r^2 - 3\chi^2}{r^5} \right\rangle \quad (89)$$

where $\chi = x,y,z$.

The Laplace equation is again satisfied and therefore

$$A_{xx} + A_{yy} + A_{zz} = 0 \quad . \quad (90)$$

The unpaired spin density at the nucleus produces an additional contribution to the hyperfine Hamiltonian, the Fermi contact term.

This will arise only from spin density in s orbitals since the other orbitals have a vanishing probability of being at the nucleus. The Fermi contact contribution is usually considered to be isotropic and is written as

$$H_{HF}^{F} = C(S_x I_x + S_y I_y + S_z I_z) \tag{91}$$

where

$$C = (8\pi/3)\gamma_e \gamma_n \hbar^2 |\psi_s(0)|^2 \tag{92}$$

and $|\psi_s(0)|^2$ is the s electron spin density at the nucleus.

The total hyperfine Hamiltonian can be written as

$$H_{HF} = A'_{xx} S_x I_x + A'_{yy} S_y I_y + A'_{zz} S_z I_z \tag{93}$$

where

$$A'_{xx} = A_{xx} + C, \text{ etc.} \tag{94}$$

If the three components of the total hyperfine Hamiltonian are measured, the contribution due to the anisotropic and isotropic components can be separated; however, the absolute signs will not generally be obtained. It should be pointed out that since the nuclei in which we are interested also have quadrupole moments, the Fermi contact term will not be strictly isotropic since the nuclei are distorted, and consequently, the dipole-dipole and contact terms are not completely separable.

D. The Total Hamiltonian, Energy Levels and Transition Probabilities

The total Hamiltonian for two molecules which are examples of the triplet state electrons interacting with an $I = 1$ and

an $I = 3/2$ nuclear spin are considered. In order to simplify the discussion we make the following assumptions for both cases:

1) The principal axis system of $H_{SS}$, $H_Q$ and $H_{HF}$ are coincident,
2) Only the out-of-plane component of the hyperfine Hamiltonian need be considered, and
3) The hyperfine interaction due to protons may be neglected.

Assumptions 1 and 2 can be, in many cases, justified on the basis of the single crystal ESR spectra[64] and assumption 3 on the fact that resolved proton hyperfine splitting has not been observed in zero field ESR.

An example of a molecule which is characterized by the interaction of one $(I = 1)$ nuclear spin with the triplet electrons is the $\pi\pi^*$ state of quinoline (1-azanaphthalene). The spin Hamiltonian for this molecule may be written as

$$H = H_{SS} + H_Q + H_{HF} \tag{95}$$

where

$$\begin{aligned} H_{SS} &= -XS_x^2 - YS_y^2 - ZS_z^2 \\ H_Q &= -xI_x^2 - yI_y^2 - zI_z^2 \end{aligned} \tag{96}$$

and

$$H_{HF} = A_{xx} S_x I_x$$

where $x$ is the out-of-plane axis.

For illustration[26] we will use for the basis states the product functions $|\mu\ \nu> = \tau_\mu\ \chi_\nu$, which form a set of eigenfunctions that

diagonalize $H_{SS}$ and $H_Q$. $\tau_\mu$ and $\chi_\nu$ are the electron and nuclear spin function while $\mu$ and $\nu$ correspond to x,y and z.

The complete Hamiltonian is, of course, a 9 x 9 matrix. Since we are only considering the $A_{xx}$ element of the hyperfine interaction,[28] a satisfactory solution is obtained by perturbation theory. As is shown in Figure 4, the energy of the states $|Zz>$ and $|Zy>$ are shifted by an amount $\beta$, where

$$\beta = \frac{A_{xx}^2}{E_y - E_z} \tag{97}$$

while the states $|Yz>$ and $|Yy>$ are shifted by an amount $-\beta$. In our axis system the triplet state energy levels would be ordered $Z > Y > X$ and the nuclear quadrupole energy levels ordered $x > z > y$. The eigenvectors of the states which are coupled by $A_{xx}$ are

$$\begin{aligned}
|Zz>' &= (1 - \beta)\,|Zz> - \beta\,|Yy> \\
|Zy>' &= (1 - \beta)\,|Zy> - \beta\,|Yz> \\
|Yz>' &= (1 - \beta)\,|Yz> + \beta\,|Zy> \\
|Yy>' &= (1 - \beta)\,|Yy> + \beta\,|Zz>
\end{aligned} \tag{98}$$

The probability for microwave transitions between the triplet state magnetic sublevels is given by

$$I \approx |<\mu_1 \nu_1 | H_{RF}(t) | \mu_2 \nu_2>|^2 \tag{99}$$

where $H_{RF}(t)$ is the magnetic dipole transition operator defined by

$$H_{RF}(t) = H_1(t)\,\hbar\,(\gamma_n \cdot I + \gamma_e \cdot S) \tag{100}$$

and $H_1(t)$ is the magnitude of the time-dependent magnetic field. The electron spin magnetic dipole transition operator will connect states with $\mu_1 \neq \mu_2$ and $\nu_1 = \nu_2$, while the nuclear spin operator will connect states with $\mu_1 = \mu_2$ and $\nu_1 \neq \nu_2$. However, *the mixing of the basis function by* $A_{xx}$ *allows the observation of "forbidden" simultaneous electron and nuclear transitions.* This is clearly shown by considering the transition from $|Xz>'$ to $|Yy>'$. The intensity of the transition is given by

$$I \approx |<Xz|\gamma_e H_1(t)|[(1-\beta)|Yy> + \beta|Zz>]|^2 \qquad (101)$$

$$I \approx \beta^2 \gamma_e^2 H_1(t)^2 \qquad (102)$$

It should be noted that it is *necessary to have a hyperfine interaction in order to observe the nuclear quadrupole satellites* since the hyperfine term is the only method of coupling the electron and nuclear spin Hamiltonians.

In Figure 5, the spectra expected for the three zero field transitions are shown in terms of the components of the total Hamiltonian. It is clear that the separation of the quadrupole satellites for both the $\tau_x \rightarrow \tau_z$ and $\tau_x \rightarrow \tau_y$ transitions is $2(z - y)$ and therefore only one of the three possible nuclear quadrupole transitions equal to $(3/4)\, e^2qQ\,(1 - \eta/3)$ is observed. The value of the hyperfine coupling constant $A_{xx}$ is easily obtained from the separation of the two allowed components of each of the three transitions. If we had

chosen to use $A_{yy}$ or $A_{zz}$ as the only hyperfine interaction instead of $A_{xx}$, the spectra would be the same as that shown in Figure 5 if a cyclic perturbation is applied to our labeling.

Although in this simple example all the parameters in the Hamiltonian can be determined from the three zero field transitions, in practice this is usually not the case. This can be due to such problems as poor resolution of the spectra or the failure to include enough terms in the Hamiltonian to adequately describe the interactions. Therefore, it is usually advantageous to also perform an electron nuclear double resonance (ENDOR) experiment to improve the resolution and confirm the assignment of the spectra. The ENDOR transitions are shown in Figure 4 by the double arrows. Let

us consider the intensity of the ENDOR transition. As an example we will treat the transition from $|Yy>'$ to $|Yz>'$

$$I \approx \left|\left[(1-\beta)<Yy| + \beta<Zz|\right] H_{RF(t)} \left[(1-\beta)|Yz> + \beta|Zy>\right]\right|^2 \quad (103)$$

$$I \approx \left[(1-\beta)^2 \gamma_n H_1 + 2\beta(1-\beta)\gamma_e H_1 + \beta^2 \gamma_n H_1\right]^2 \quad (104)$$

Since $H_1$ is a constant, we will drop it and may now write

$$I \approx 4\gamma_e^2\left[\beta^2(1-\beta)\right] + 4\gamma_e\gamma_n\left[\beta(1-\beta)^3 + \beta^3(1-\beta)\right] + \gamma_n^2\left[(1-\beta)^4 + \beta^4 + 2\beta^2(1-\beta)^2\right] \quad (105)$$

Since $\beta$ is usually on the order of $1 \times 10^{-2}$ for $\pi\pi^*$ triplets, we can reasonably approximate Equation 64 by

$$I \approx 4\beta^2 \gamma_e^2 + 4\beta \gamma_e \gamma_n + \gamma_n^2 \qquad (106)$$

In contrast, if there were no hyperfine coupling as in the $\tau_x$ manifold in our example, the intensity would be given by

$$I \approx \gamma_n^2 \quad . \qquad (107)$$

The ratio of the intensity of the ENDOR transitions due to the electron magnetic dipole operator to those due to the nuclear magnetic dipole operator is approximately $4\beta^2 \gamma_e^2/\gamma_n^2$ and therefore, unless $\gamma_n^2$ is greater than $4\beta^2\gamma_e^2$ the electron dipole moment transition operator will be the major source of the intensity in ENDOR transitions.

As an example, for $^{14}N$ the ratio of $\gamma_e/\gamma_n = 8.6 \times 10^6$ and therefore, $\beta$ must be less than $1.57 \times 10^{-3}$ for the nuclear magnetic dipole transition operator to be comparable to the electron magnetic dipole transition operator in producing intensity in the ENDOR transitions. For a typical separation of $\tau_z - \tau_y$ of 1000 MHz this would correspond to an extremely small hyperfine element, $A_{xx}$ of only 1.5 MHz, which is much smaller than any out-of-plane hyperfine elements reported for aza-aromatics.

As an example of a molecule with one I = 3/2 nuclear spin, we will consider the excited $^3\pi\pi^*$ state of chlorobenzene. The spectrum produced in this case is somewhat more complicated to calculate because of the lack of a convenient

basis set for both the electron and nuclear spin functions. The simplest method with only one hyperfine component is to use the basis set $|\mu\ \nu\rangle$ $\tau_\mu\ \chi_\nu$ where $\mu$ corresponds to X, Y and Z and $\nu$ to 3/2, 1/2, -1/2 and -3/2. We will further assume that $\eta = 0$ and therefore both $H_{SS}$ and $H_Q$ are again diagonal. In this example the out-of-plane component of the hyperfine tensor $(A_{xx})$ couples the basis states in the $\tau_z$ manifold with those in the $\tau_y$ manifold for which the nuclear spins differ in their $I_z$ quantum number by $\pm 1$. This is easily seen by expanding the hyperfine Hamiltonian as

$$A_{xx} S_x I_x = 1/2\left[A_{xx} S_x (I_+ + I_-)\right] \quad . \tag{108}$$

The states in the Hamiltonian that are coupled by $A_{xx}$ may be represented graphically as

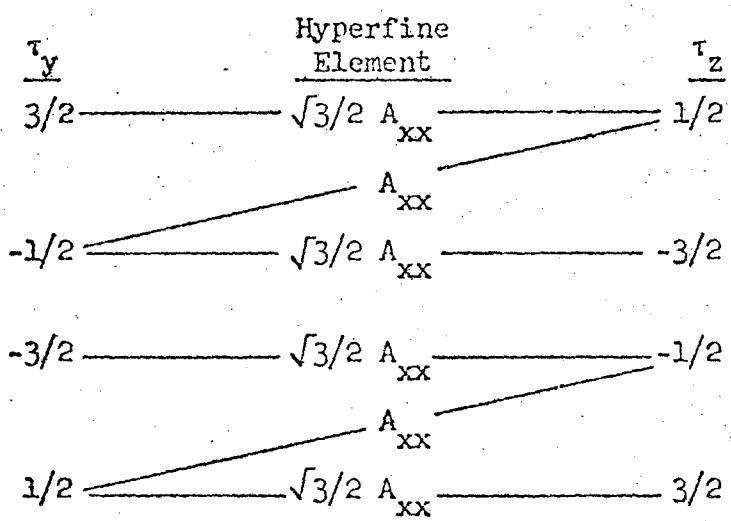


Since the degenerate nuclear levels are not coupled by the same hyperfine element, we may still use non-degenerate perturbation theory to calculate the energy levels and transition moments.

This spin system has a total spin that is a half integer (5/2), it is a Kramers doublet, and therefore all the energy levels are two-fold degenerate. The hyperfine coupling will never remove the degeneracy of the ± nuclear levels in zero field and consequently we have only six levels to consider.

The energy level diagram resulting from a perturbation treatment of the hyperfine interaction is given in Figure 6, and the predicted spectra in Figure The use of the $A_{yy}$ component of the hyperfine tensor instead of the $A_{xx}$ component produces an identical energy level diagram and spectra with the appropriate relabeling. The use of the $A_{zz}$ component of the hyperfine tensor mixes the nuclear sublevels in the $\tau_x$ manifold with those in the $\tau_y$ manifold having the same $I_z$ quantum number,

| $\tau_x$ | Hyperfine Element | $\tau_y$ |
|---|---|---|
| 3/2 | 3/2 $A_{zz}$ | 3/2 |
| 1/2 | 1/2 $A_{zz}$ | 1/2 |
| -1/2 | -1/2 $A_{zz}$ | -1/2 |
| -3/2 | -3/2 $A_{zz}$ | -3/2 |

therefore, no nuclear quadrupole satellites due to the electron magnetic moment transition operator are observed. The resulting energy level diagram, considering only the $A_{zz}$ component of the hyperfine tensor is given in Figure 8 and the predicted spectra in Figure 9.

The ENDOR transitions permitted by the electron dipole moment transition operator, considering only the $A_{xx}$ hyperfine element,

are shown by the double arrows in Figure 6. The analysis of the ENDOR spectra follows the same method as that for a spin one nucleus, with the same expression for the intensity of the transitions induced by the electron magnetic dipole moment transition operator and the nuclear magnetic dipole moment transition operator. When only the $A_{zz}$ hyperfine element is present, the electron magnetic dipole transition operator is ineffective in producing ENDOR transitions and consequently the intensity of any observed ENDOR signal is due solely to the nuclear magnetic dipole transition operator.

Some generalizations can be made at this point concerning the appearance of "forbidden"satellites whose separation is in the zeroth order is the pure nuclear quadrupole transition frequency of the molecules in an excited triplet state. (a) *For a nuclear spin* I = 1 (e.g. $^{14}N$), *a hyperfine element,* $A_{ii}$, *associated with a direction* i *gives intensity into a simultaneous electron-nuclear flip in the plane normal to* i. *Thus at least two nuclear hyperfine elements must be finite to obtain independently both* $e^2qQ$ *and* $\eta$. (b) *For a nuclear spin* I = 3/2 (e.g. $^{35}Cl$), *a nuclear hyperfine element parallel to the principal axis of the field gradient* (i.e., $A_{zz}$) *does not introduce mixing between electron-nuclear states that admit intensity into forbidden satellites.* (c) *For a nuclear spin* I = 3/2, *a nuclear hyperfine element perpendicular to the principal axis of the field gradient introduces intensity into forbidden satellites whose separation in zeroth order is the pure nuclear quadrupole transition frequency; however,* $e^2qQ$ *and* $\eta$ *can never be obtained independently in the absence of an external magnetic field.* Although we will not discuss the observation in any detail, we should point out that in many cases it is possible to obtain the sign of the nuclear quadrupole moment from an analysis of the zerofield spectra. This feature is

discussed fully in Reference (78).

Although we have not treated explicitly the case where two nuclei are present on the same molecule, both having nuclear spin $I \geq 1$, the generalizations (a)-(c) hold with one additional feature being manifested, that is the possibility of simultaneous multiple nuclear-electron spin flips. As we will see in the following sections, in 8-chloroquinoline, simultaneous chlorine-nitrogen electron spin transitions are observed and are easily identified. In addition simultaneous multiple nuclear ENDOR transitions are expected and, indeed, observed.

## IV. EXPERIMENTAL METHODS

### A. Optically Detected Magnetic Resonance

The basic experimental arrangement is shown in Figure 10. The sample is mounted inside a helical slow wave structure[65] which is attached to a rigid stainless steel coaxial line suspended in a liquid helium dewar. The exciting light is supplied by a 100-watt mercury short arc lamp. The spectral region of interest selected by either an interference filter centered at 3100 Å, or a combination of Corning glass and solution filters.[66] The phosphorescence is collected at a 90° angle to the exciting light and is focused through an appropriate Corning filter (to remove scattered light) onto the entrance slit of a Jarrel-Ash 3/4 meter spectrometer. The light at the exit slit is detected with an EMI 6256S photomultiplier cooled to -20°C. whose output is connected to an electrometer through an adjustable load resistor. The output of the

electrometer is either monitored directly if c.w. microwave power is used, or if the microwave field is amplitude modulated, connected to the signal channel input of a PAR model HR-8 lock-in amplifier.

The microwave field is generated by a Hewlett-Packard microwave sweep oscillator Model 8690B, amplified with a traveling wave tube and fed consecutively through a directional coupler, band-pass filter, and an isolator to the rigid coaxial line to which the helix is mounted. The microwave sweep oscillator may be amplitude modulated with a square wave generator which is also connected to the reference channel of the lock-in amplifier. The output of the lock-in amplifier drives the y axis of an x-y recorder while the ramp voltage from the microwave sweep oscillator drives the x axis.

The temperature of the sample is usually lowered to approximately 1.3$^{o}$K by pumping on the liquid helium with three Kinney model KTC-21 vacuum pumps operated in parallel.

The experiment is performed by monitoring the change in emission of the sample while varying the frequency of the modulated microwave field. As explained in section II, the signal may either increase or decrease. With a lock-in amplifier a decrease in emission intensity corresponds to a phase shift of 180 degrees relative to the signal obtained for an increase in emission intensity.

B. Optically Detected ENDOR

The experimental arrangement usually employed is shown in Figure 11. The optical and microwave equipment is the same as that used in the ODMR experiments with the exception that the microwave field ($H_1$) is not modulated. The radiofrequency field ($H_2$) is supplied by a sweep oscillator that covers the region from 0.1 to 110 MHz. The output is modulated by a

linear gate that is driven by a square wave generator which also drives the reference channel of the lock-in amplifier. The RF is then amplified by two broad-band distributed amplifiers, a 4 watt unit and a 20 watt unit, and connected to the ENDOR coils. These amplifiers have the advantage that they operate over the range of 1 to 50 MHz without the need of adjustment. The ENDOR coil consists of a "bridge T" constant resistance network in a Helmholtz arrangement. This configuration maintains an even rf level over a broad-band of frequencies since it looks entirely resistive. The x axis of the recorder is driven by the ramp voltage from the rf sweep oscillator and the y axis from the output of the lock-in amplifier.

C. Variations of the Basic Experiments

The optical detection of magnetic resonance permits several additional parameters to be experimentally adjusted. These include the energy and bandwidth of the phosphorescence that is monitored as well as the energy, bandwidth and intensity of the exciting light. In addition, the power of the microwave field $H_1$ may be adjusted over a wider range than in experiments in which the absorption of microwave power is monitored. This is due to the fact that saturation gives the maximum signal strength using optical detection techniques, while with absorption experiments the signal strength will decrease as the power is increased above that needed for saturation. The advantage of this is that the signal strength of weak "forbidden" transitions may be improved by the application of large $H_1$ fields without a decrease in the signal strength of the allowed transitions.

Some of the most useful variations of the basic experiment are listed in Table IV. If a high resolution spectrometer is employed to isolate the phosphorescence emission, the optically detected ESR may be

used to simplify the phosphorescence spectrum by amplitude modulation of the $H_1$ field while saturating an ESR transition. The modulation of the phosphorescence is detected with a phase sensitive amplifier while sweeping the optical spectrum. Since only two of the three triplet levels are coupled by the $H_1$ field, only the emission from these two levels will be detected. Therefore, by repeating the experiment while saturating the remaining two ESR transitions, three PMDR spectra are obtained, each including only the emission from two of the three zero field levels. The information obtained from the analysis of phosphorescence spectra is extremely useful by itself in characterizing the triplet state, and complementary to the information obtained from the analysis of the ESR spectrum.

In ENDOR experiments the radiofrequency field $H_2$ may also be adjusted. These experiments are usually performed by saturating an ESR transition while varying the frequency of the $H_2$ field. Either the $H_1$ or $H_2$ fields may be modulated; however, it is usually preferable to modulate the $H_2$ field since, in this case, only the change in intensity of the phosphorescence due to the ENDOR resonance is detected with a lock-in amplifier. On the other hand, if the $H_1$ field is modulated, there is a constant signal due to the ESR transition which changes in intensity when the $H_2$ field is swept through resonance. A useful modification of this technique is achieved by modulation of the $H_2$ field while simultaneously saturating an ENDOR transition and sweeping the $H_1$ field. In this case, only the ESR transitions that connect energy levels simultaneously coupled by the $H_1$ and the $H_2$ fields are detected. This method is useful in analyzing the structure of the ESR transition since the contribution to the spectrum due to different isotopes and/or nuclei may be isolated.

If both an ESR and an ENDOR transition are saturated while modulating the $H_2$ field and scanning the phosphorescence spectrum, it is possible to isolate the contribution to the phosphorescence spectrum from molecules containing different nuclear isotopes. As an example, if the phosphorescence from a molecule such as chlorobenzene is monitored and a $Cl^{35}$ ENDOR transition saturated while modulating the $H_2$ field, only the contribution to the phosphorescence spectrum from molecules containing the $Cl^{35}$ isotope will be detected. The same experiment may then be repeated detecting only the contribution from the molecules containing the $Cl^{37}$ isotope.

V. The ODMR Spectra of 8-chloroquinoline

The zero field spectra of 8-chloroquinoline is characterized by the interaction of the triplet electrons with both a nitrogen (I=1) and a chlorine (I=3/2) nucleous. The addition of the chlorine atom to quinoline does not appreciably change the lifetime of the phosphorescence (see Table 2). Both quinoline and 8-chloroquinoline show emission primarily from only one of the triplet sublevels and have essentially the same zero field, nitrogen quadrupole and nitrogen hyperfine interactions.

Although a great deal of information concerning the pathway of intramolecular energy transfer (i.e., intersystem crossing, radiative rate processes, etc.) can be obtained from an analysis of the microwave-induced phosphorescence intensity changes, we will restrict the results and discussion to the salient features of the ODMR spectra in zero field.

Two of the three electron spin transitions, those associated with the $\tau_z \rightarrow \tau_y$ and $\tau_x \rightarrow \tau_y$ manifolds were observed with both a continuous microwave field while monitoring the intensity of the phosphorescence and with 5 Hz amplitude modulation of the microwave field and phase sensitive detection of the component of the phosphorescence at the modulation frequency. The $\tau_x \rightarrow \tau_z$ transition was only observed in an EEDOR experiment. This was performed by simultaneously saturating the $\tau_x \rightarrow \tau_y$ transition with a c.w. microwave field and amplitude modulation of a second microwave field which was swept through the $\tau_x \rightarrow \tau_z$ transition. This was necessary since emission originates almost entirely from only the $\tau_y$ spin manifold. In all cases the phosphorescence intensity increased when the microwave field coupled the respective electron spin manifolds. The lifetime of the emission from the $\tau_y$ manifold was found to be 0.11 sec.

while the lifetimes of both $\tau_x$ and $\tau_z$ levels are each more than one second. With the assumption that the radiative lifetimes of the triplet levels are ordered the same as the total lifetimes and the observation that the phosphorescence intensity increased while saturating both the $\tau_x \rightarrow \tau_y$ and $\tau_z \rightarrow \tau_y$ spin manifolds, from Equation 147 the steady state population of the $\tau_y$ level must be less than the population of either the $\tau_x$ or the $\tau_z$ levels. The spectra obtained with amplitude modulation of the three ESR transitions are shown in Figure 12. At low microwave powers only the "allowed" component of each spectrum was observed. As the microwave power was increased, "forbidden" satellites split off the major transition were observed. The $^{35}$Cl ENDOR resonance observed while saturating the $\tau_z \rightarrow \tau_y$ transition is shown in Figure 13. This transition was also observed with both a continuous and amplitude modulated rf field.

The phosphorescence of 8-chloroquinoline in durene is due to the two distinct sites,[67] the more intense phosphorescence origin at 4795 Å and a weaker origin at 4792 Å. In order to isolate the emission from the site at 4795 Å, the ODMR spectra were obtained with the entrance slit of the spectrometer adjusted to 100 microns or less.

The ODMR spectra observed may be considered as due to two distinct molecular isotopes since approximately 75% of the 8-chloroquinoline molecules will have the $^{35}$Cl isotope and 25% the $^{37}$Cl isotope. We will initially limit our consideration to only the 8-chloroquinoline molecules that have the $^{35}$Cl isotope. The molecular axis system we will use is defined with x, the out-of-plane axis; y, the long in-plane axis; and z, the short in-plane axis. In order to simplify the analysis of the spectra, we will make the following assumptions:

(1) The contribution of the proton hyperfine interactions will be neglected.

(2) The principal axis systems of the spin-spin, nuclear quadrupole, and hyperfine interactions are coincident.

(3) Only the out-of-plane hyperfine element for both nitrogen and chlorine will be considered.

(4) The chlorine asymmetry parameter is assumed to be zero.

The first assumption is justified on the basis of the small contribution to the linewidth reported by Hutchison et al.[68] due to the proton hyperfine interaction in zero field. This effect is smaller than the other terms in the Hamiltonian and would require an extensive computer analysis and excellent resolution of the transitions to justify its considerations.

The second assumption is quite severe, but is reasonable for our purposes since slight non-coincidence of the tensor elements will only produce a small perturbation of the observed spectra in zero field. In addition, the x axis is fixed by symmetry to be perpendicular to the plane and in quinoline it has been found that the z axis of $H_{SS}$ is within a few degrees of the molecular z axis.[64, 69] It is also reasonable to expect the principal nuclear quadrupole axis for both the nitrogen and chlorine atoms to be along the molecular z axis.[63]

The third assumption is based on the measured value for the nitrogen hyperfine interaction for the excited triplet state of quinoline for which $A_{xx} \gg A_{yy}, A_{zz}$,[64] and on the observation of chlorine hyperfine interactions in organic free radicals in which the principal chlorine hyperfine element has been found to be the out-of-plane element.[70, 71] In addition, since in zero field the hyperfine interaction is an off-diagonal term in the spin Hamiltonian, the magnitude of the effect of the interaction on the observed spectra is in first order inversely proportional to the energy separation of the triplet manifolds that are connected by the respective hyperfine element. In the case of 8-chloroquinoline even if the hyperfine interaction was isotropic, the effect on the zero field spectra would still be three times larger for the $A_{xx}$ than the $A_{yy}$ or $A_{zz}$ components. Therefore, only the $A_{xx}$ component of the hyperfine tensor will be included for both the chlorine and nitrogen atoms since this will account for the major features of the spectra.

The fourth assumption is made on the basis that a finite value of the chlorine asymmetry parameter is a small perturbation that is not easily resolvable and not necessary to explain the main features of the spectra.

With these assumptions, the spin Hamiltonian may be written

$$H = H_{SS} + H_Q^N + H_{HF}^N + H_Q^{Cl} + H_{HF}^{Cl} \qquad (109)$$

where

$$\begin{aligned} H_{SS} &= -XS_x^2 - YS_y^2 - ZS_z^2 \\ H_Q^N &= -xI_x^2 - yI_y^2 - zI_z^2 \\ H_{HF}^N &= A_{xx}^N(S_xI_x) \\ H_Q^{Cl} &= \frac{e^2qQ}{12}\left[3I_z^2 - \frac{15}{4}\right] \\ H_{HF}^{Cl} &= A_{xx}^{Cl}(S_xI_x) \end{aligned} \qquad (110)$$

In the same manner as discussed in section III-D the basis states of the spin Hamiltonian are chosen to be the product functions $|u,v,w\rangle = \tau_u, \chi_v, \chi_w$, which diagonalizes $H_{SS}$, $H_Q^N$ and $H_Q^{Cl}$. $\tau_u$ $(u = x,y,z)$ is the electron spin function, $\chi_v$ $(v = x,y,z)$ is the nitrogen spin function and $\chi_w$ $(w = \pm 1/2, \pm 3/2)$ is the doubly degenerate chlorine spin function. The total spin of the system is 7/2 and therefore a Kramers doublet; consequently, there are only 18 energy levels for each of the molecular isotopes.

The similarity of the excited triplet state of 8-chloroquinoline and quinoline leads to the assignment of the order of the triplet energy levels of 8-chloroquinoline as being the same as those of quinoline.[72] With our axis system, the elements of $H_{SS}$ are ordered $Y > Z > X$. The nitrogen nuclear quadrupole energy levels are also assumed to be in the same order as those reported for the ground state of pyrazine and pyridine[73, 74] and thus for $H_Q^N$, $x > y > z$.

Since the chlorine nuclear quadrupole coupling constant ($e^2qQ$) is negative for all covalently bonded Cl atoms, the energy of the chlorine spin functions are ordered $\chi_{\pm 1/2} > \chi_{\pm 3/2}$.

In order to treat the out-of-plane hyperfine perturbation due to both the nitrogen and chlorine spins, we will assume that the contribution from each may be considered separately. This is of course not strictly correct, but is satisfactory for the purpose of illustration, and in fact, for the value of $A_{xx}^{N}$ and $A_{xx}^{Cl}$ used in fitting the spectra, gives values for the energy levels very close to those obtained by diagonalizing the total spin Hamiltonian.

An energy level scheme using the perturbation method discussed in section III-D appropriate for 8-chloroquinoline is given in Figure 14. There are essentially six types of ESR transitions observed:

A) electron spin,

B) electron and $^{14}N$ spins,

C) electron and $^{35}Cl$ spins,

D) electron and $^{37}Cl$ spins

E) electron, $^{14}N$ and $^{35}Cl$ spins

F) electron, $^{14}N$ and $^{37}Cl$ spins.

Since the chlorine nuclear quadrupole interaction is far larger than the nitrogen nuclear quadrupole interaction, the various types of transitions are easily identified. In Table 3 the measured and calculated frequencies are listed according to their type (A,B, etc.). In analyzing the spectra, the magnitude of the components of the spin Hamiltonian were first obtained by perturbation theory and the final results by computer

diagonalization of the spin Hamiltonian. The $^{14}N$ and $^{35}Cl$ out-of-plane hyperfine elements were found to be approximately 19.5 and 15 MHz respectively. With only one nitrogen hyperfine element only one nitrogen quadrupole transition is observed corresponding to the in-plane $\chi_z \rightarrow \chi_y$ transition which was found to be 3.2 ± .2 MHz. With our assumption that the asymmetry parameter may be neglected the $^{35}Cl$ nuclear quadrupole coupling constant was found to be -68.4 ± 0.6 MHz.

The calculated frequencies listed in Table 3 were obtained by analysis of the components of the observed spectra due to the $^{35}Cl$ molecular isotope. The transitions associated with the molecules possessing the $^{37}Cl$ isotope were then obtained by using the same values for $H_{SS}$, $H_Q^N$ and $H_{HF}^N$ and correcting $H_Q^{Cl}$ for the difference in the nuclear quadrupole moments and $H_{HF}^{Cl}$ for the difference in the magnetogyric ratio of the two chlorine isotopes. All calculated frequencies were obtained by collecting all transitions within 0.75 MHz of another and weighting each by its electron magnetic moment transition probability.

It is difficult to make a comprehensive analysis of the electron distribution in the excited triplet state without a measure of all the components of the hyperfine tensor. The similarity of the nitrogen nuclear quadrupole and hyperfine interactions in 8-chloroquinoline and quinoline and the observation that the chlorine nuclear quadrupole coupling constant is approximately the same as that reported for the ground state of 6-chloroquinoline (69.256 MHz)[75] and 7-chloroquinoline (69.362 MHz)[71] supports the assumption that the excited triplet state of 8-chloroquinoline is essentially the same as that of quinoline.

VI. The ODMR Spectra of Paradichlorobenzene

A detailed analysis of the ODMR spectra of paradichlorobenzene (DCB) has been previously reported.[29] In this section those results are summarized with special attention to the determination of the chlorine nuclear quadrupole coupling constant. The DCB ODMR spectra is a function of the particular trap emission monitored and the host material. We will limit this discussion to the shallow trap emission in neat DCB.

As was the case with 8-chloroquinoline, the observed ODMR spectra of DCB is due to the interaction of isotopically distinct molecular species. The fractional natural abundances of the $^{35}Cl$ and $^{37}Cl$ isotopes are approximately 3/4 and 1/4, respectively. Since there are two chlorine nuclei per molecule, the fractional distribution of the molecular species are:

| | | |
|---|---|---|
| I | $^{35}Cl - ^{35}Cl$ | = 9/16 |
| II | $^{35}Cl - ^{37}Cl$ | = 6/16 |
| III | $^{37}Cl - ^{37}Cl$ | = 1/16. |

The spectra are treated as a weighted superposition of the ODMR spectra due to each of the three molecular species.

The $\tau_x \rightarrow \tau_y$ (high frequency) transitions observed using amplitude modulation is shown in Figure 15. The remaining two electron spin transitions ($\tau_x \rightarrow \tau_z$ and $\tau_z \rightarrow \tau_y$) have essentially the same structure as the spectra illustrated for the $\tau_x \rightarrow \tau_y$ transition; however, the signal-to-noise ratio of the $\tau_z \rightarrow \tau_y$ transition was substantially lower.

In Table 4 the possible ESR transitions involving the triplet electrons and one or more chlorine nuclei are listed as to type (A,B,C, D,E, or F) and the molecular species (I, II or III) which can undergo each type of transition. The intensity of the transitions involving the

electron and one chlorine spin (B and C) and those involving the electron and two chlorine spins (D, E and F) must be considered separately. The ratio of the intensities of the transitions involving a single $^{35}Cl$ spin (type B) to those involving a single $^{37}Cl$ spin (type C) should be three to one on the basis of the ratio of $^{35}Cl$ to $^{37}Cl$. The ratio of the intensities of the transitions involving two chlorine spins is likewise $I_D:I_E:I_F = 9:6:1$.

The structure of the $\tau_x \rightarrow \tau_y$ electron spin multiplet shown in Figure 15 is labeled according to the classification given in Table 1. Since the nuclear quadrupole moment of $^{35}Cl$ is larger than that of $^{37}Cl$ the outer pair of the four strong satellites are assigned as type B ( $^{35}Cl$) and the inner pair as type C transitions ($^{37}Cl$). As can be seen, the ratio of the intensity of the transitions labeled B and C is approximately 3:1 as predicted. The outermost satellites in Figure 15 are assigned to simultaneous double chlorine transitions (labeled D and E on the spectra). The intensity of these transitions is approximately in the predicted ratio of 9:6. The transitions corresponding to simultaneous double $^{37}Cl$ transitions (type F) are not observed consistent with the small natural abundance of the molecular species responsible for these transitions. The inner pair of satellites (labeled E in Figure 15) may be considered as simultaneous electron and $^{35}Cl$ and $^{37}Cl$ transitions. The higher frequency satellite represents a simultaneous electron spin transition, a $^{35}Cl$ $(\pm\frac{3}{2} \rightarrow \pm\frac{1}{2})$ and a $^{37}Cl$ $(\pm\frac{1}{2} \rightarrow \pm\frac{3}{2})$ transition while the lower frequency satellite represents the opposite chlorine transitions. These transitions are separated by the difference between the $^{35}Cl$ and $^{37}Cl$ nuclear quadrupole coupling constants. Naturally these occur for only those

molecules that have one $^{35}Cl$ and one $^{37}Cl$ isotope. Since the matrix elements for these double chlorine transitions are of a different form than those associated with the other double chlorine transitions, the intensity of the inner satellites labeled E in Figure 15 may not be compared directly with the intensity of the outer satellites labeled D and E. All transitions involving both an electron and a nuclear spin

required several orders of magnitude greater microwave power to obtain intensities comparable to the electron only (type A) transition. Chlorine nuclear transitions were observed via optically detected ENDOR by saturating the ESR transitions associated with the $\tau_x \rightarrow \tau_y$ or $\tau_x \rightarrow \tau_z$ manifolds. Both the $^{35}Cl$ and $^{37}Cl$ ENDOR resonances were observed while saturating either ESR transition. Figures 16a and 16b illustrate the $^{35}Cl$ ENDOR resonances associated with the $\tau_x \rightarrow \tau_y$ and $\tau_x \rightarrow \tau_z$ transitions, respectively.

As an extension of the ENDOR experiments a $^{35}Cl$ ENDOR transition was saturated while sweeping the $\tau_x \rightarrow \tau_z$ microwave transition. Since only the ENDOR time dependent magnetic field was amplitude modulated and the change in phosphorescence intensity detected with a lock-in amplifier only the ESR transitions that involve at least one $^{35}Cl$ spin transition were detected. The spectrum obtained from this experiment is shown in Figure 17. As would be expected, satellites assigned as simultaneous electron and $^{37}Cl$ spin transitions (labeled C in Figure 15) are not observed. Finally, all measured frequencies associated with the three electron spin

zero-field transitions are given in Table 6, while the $^{35}Cl$ and $^{37}Cl$ ENDOR transitions are listed separately in Table 7.

Following the discussion in Section III the observed spectra are explained in terms of a Hamiltonian of the form:

$$H = H_{SS} + \sum_i H_Q + \sum_i H_{HF} \qquad (111)$$

where the summation is over the chlorine nuclei and $H_{HF} = A_{xx} S_x I_x$. The ODMR spectra were simulated by use of a computer program that diagonalized the spin Hamiltonian and calculated the transition frequencies and intensities. The spin Hamiltonian parameters used in simulating the spectra observed while monitoring the x-trap emission are listed in Table 5 along with the approximate values of $H_{SS}$ for the y trap and the values reported for benzene.[79] The best value obtained for the $^{35}Cl$ nuclear quadrupole coupling constant was -64.50 MHz ($^{37}Cl$ = -50.84 MHz) and for the $^{35}Cl$ hyperfine interaction $A_{xx}$ = 22 MHz ($^{37}Cl$: $A_{xx}$ = 18.3 MHz). The experimental and calculated ESR frequencies for the x trap of DCB are listed in Table 6. With the parameters used in the spin Hamiltonian all of the calculated transition frequencies are within experimental error. However, a small error in the calculated frequencies is introduced since a weighted average of the transitions corresponding to a particular type was made.

The observed and calculated chlorine ENDOR transitions associated with the $\tau_x \rightarrow \tau_y$ and $\tau_x \rightarrow \tau_z$ multiplets are listed in Table 7. Because of the large linewidth of the observed ENDOR transitions and because many ENDOR transitions are expected in a small range of frequencies it is difficult to explicitly assign the observed spectra to any particular calculated transition. An additional complication arises when one considers the transition moments associated with the individual transitions. Since they

vary, one should weight the calculated spectra according to the square of the ENDOR transition moments and compare these spectra with the observed. However the observed spectra are obtained under saturating conditions, and therefore intensities are practically meaningless. We compared only the range of calculated ENDOR frequencies listed in Table 4 with the experimental results.

From a second order perturbation analysis of the DCB ODMR spectra[78] it has been shown that with the assumption that $e^2qQ$ is negative, D is positive or x < z, y. This result is entirely consistent with previous experimental[11,79] and theoretical[61] studies of aromatic molecules in $\pi\pi^*$ triplet states. Indeed this is what is observed for the lowest $\pi\pi^*$ triplet state of benzene.[77] The ordering of the interaction along the two in-plane molecular axis is however not immediately apparent. From the analysis of the spectra of DCB utilizing phosphorescence microwave double resonance (PMDR) spectroscopy the component of the electron spin-spin interaction along the molecular y (or short in-plane axis) has been assigned as the larger of the two in-plane components of the electron spin-spin tensor.[39]

Since the zero-field splitting parameters D and D* ($D^* = (D^2 + 3E^2)^{\frac{1}{2}}$) are primarily a function of the size of the $\pi$ system involved in the excitation,[62] the value of these parameters for both DCB and benzene should be similar if DCB is a $\pi\pi^*$ triplet. As can be seen in Table 5 the values of D and D* for both traps of DCB differ from the corresponding values for benzene by only a few percent which is strong confirmation of the assignment of the excited triplet state of DCB as a $\pi\pi^*$ state. The

zero-field splitting parameter E which is a measure of the anisotropy of the triplet electron distribution in the molecular plane is, however, quite different for both molecules. If the benzene molecule possessed $D_{6h}$ symmetry in the excited state, E must be zero by symmetry. The finite value of E for benzene has been explained by de Groot and van der Waals on the basis of a distortion of the benzene ring from the $D_{6h}$ to $D_{2h}$.[59,77]

A quantitative analysis of the E value of DCB is difficult since accurate wavefunctions are not available for the chlorines. However, from a simple consideration of the perturbation of the triplet electron distribution in benzene due to the addition of two para-chlorines, it is expected that the $\tau_z$ level will be lowered and the $\tau_y$ level raised in energy. Since the E value of DCB is larger than the E value of benzene, this model predicts that in DCB the $\tau_y$ level is higher in energy than the $\tau_z$ level. This of course gives the opposite sign of E for DCB as compared to benzene, and is consistent with the ordering of the triplet energy levels previously obtained from analysis of the phosphorescence microwave double resonance spectra. It is interesting to note that in 1,2,4,5 tetrachlorobenzene (TCB) the inclusion of chlorine interactions would predict the $\tau_z$ level to be higher in energy than the $\tau_y$ level; consequently, the E value would have the same sign as benzene. Other substituted chlorobenzenes should have E values between DCB and TCB. The importance of the zero-field splitting of DCB and TCB is that the presence of the chlorines acting as perturbations on the excited state of benzene raises the possibility that the symmetry of the excited state of DCB and TCB is different than that of the excited state of benzene. As has

been discussed[39] the sign of E in part answers this interesting question.

The absolute value of the chlorine nuclear quadrupole coupling constant ($e^2qQ$) in the excited state of DCB is significantly reduced compared to the corresponding value for the ground state. With the assumption that the asymmetry parameter ($\eta$) may be neglected, the value of $e^2qQ$ for the $^{35}Cl$ nuclei of DCB in its excited triplet state at $1.3^{\circ}K$ is -64.5 MHz. The measured pure nuclear quadrupole resonance frequency of DCB in its ground state at $4.2^{\circ}K$ is 34.831 MHz[29] which, if $\eta$ is assumed to equal zero, corresponds to a value of $e^2qQ$ of -69.662 MHz. The assumption that $\eta$ may be neglected is justified on the basis that $e^2qQ$ is not changed significantly for small values of $\eta$ and for the ground state of DCB at room temperature $\eta$ is only 0.08.[80] Indeed, from the explicit dependence of $e^2qQ$ on the assumption that $e^2qQ$ is simply twice the pure NQR transition frequency causes a positive error in $e^2qQ$ of less than 5% for $\eta \leq 0.5$. The increase of 52 KHz in the pure NQR frequency of the ground state of DCB upon lowering the temperature of the sample from $77^{\circ}K$ ($\nu$ = 34.779 MHz) to $4.2^{\circ}K$ ($\nu$ = 34.831 MHz) is consistent with Bayer's theory[81] which treats the temperature dependence of the NQR frequency in terms of the molecular torsional motions. More important, however, is the fact that the small change in the pure NQR transition frequency indicates that there is no major physical change in the environment of the chlorine nuclei in DCB upon cooling. Therefore, the difference in $e^2qQ$ between the ground and excited states of DCB is clearly due to a change in the electric field gradient (q) at the chlorines upon excitation. The magnitude of the decrease in the absolute value of $e^2qQ$ upon excitation is interesting

because: a) the absolute value of $e^2qQ$ in the triplet state of DCB is significantly less than the value reported for the ground state of any chlorine bonded to an aromatic molecule;[63] and b) the decrease in $|e^2qQ|$ upon excitation to the lowest $^3\pi\pi^*$ state of 8-chloroquinoline[28] and 1,2,4,5 tetrachlorobenzene[42] is far less than the decrease in $|e^2qQ|$ for DCB.

In contrast to the electron spin-spin and hyperfine interactions which are a function of only the triplet electrons, $e^2qQ$ is dependent upon the distribution of all electrons. Since electrons in s orbitals have spherical symmetry, they do not contribute to the field gradient. A closed p shell also contributes nothing to the field gradient, and following the analysis of Bersohn[82] the field gradient in DCB can be considered as arising from a hole in the chlorine $p_z$ orbital and a partial hole in the chlorine $p_x$ orbital. The total contribution is due to two axially symmetric tensors whose major axes are perpendicular. In Table 8 the contributions to the field gradient are expressed in terms of the number of holes in the $p_x$ and $p_z$ chlorine orbitals. The difference in $e^2qQ$ for the excited and ground state may be written,

$$\Delta e^2qQ = e^2(q_T - q_G)Q \qquad (112)$$

where $q_T$ and $q_G$ refer to the field gradient at the chlorines in the triplet and ground states of DCB respectively. Equation 112 may be expressed in terms of the number of holes in the $p_z$ and $p_x$ orbitals as

$$\Delta e^2qQ = e[\sigma_T-\sigma_G] - \frac{1}{2}[\delta_T-\delta_G]Q \qquad (113)$$

where $\sigma_T$ and $\sigma_G$ are the fraction of $p_z$ electron holes in the carbon-chlorine sigma bond in the triplet and ground state, respectively, while $\delta_T$ and $\delta_G$

are the fraction of $p_x$ electron holes in the $\pi$ bond for the triplet and ground states, respectively. Since $\Delta e^2qQ$ is negative, one of the following conditions must be met: a) $\sigma_G > \sigma_T$, or b) $\delta_T > \delta_G$. If $\sigma_G$ is greater than $\sigma_T$, the number of holes has decreased along the carbon-chlorine bond, and therefore the chlorine nuclei are more successful in competing for electrons in the excited state. However since the sigma electrons are not involved in the excitation, this effect should be very small. If $\delta_T$ is greater than $\delta_G$, the out-of-plane chlorine $p_x$ orbital has lost electrons. An increase in the number of holes in the $p_x$ orbital would be the most likely explanation of the decrease in $e^2qQ$ since the chlorine $p_x$ orbitals are allowed by symmetry to interact with the carbon $p_x$ orbitals. The increase in the number of holes in the chlorine $p_x$ orbital can come about from either an increase in the double bond character of the C-Cl bond or a "bent" C-Cl bond. Bray, Barnes and Bersohn[80] has shown that although the overlap of the carbon and chlorine $p_x$ orbitals is reduced with a bend C-Cl bond, the chlorine $p_x$ orbitals may overlap with the sigma system, consequently increasing the number of holes in the $p_x$ orbital of chlorine ($\delta_T$) relative to the number of holes in the $p_x$ orbital in the ground state ($\delta_G$). Although it is not possible a priori to distinguish between these two possibilities the interpretation of the change in $e^2qQ$ as arising from a bent C-Cl bond is reasonable in view of other experimental results.

The phosphorescence of DCB to the ground state in the O-O band is from all three triplet levels which requires that DCB has less than $D_{2h}$ symmetry in its $^3\pi\pi^*$ state.[39] Finally the measured value of the out-of-plane chlorine hyperfine interaction for the $^3\pi\pi^*$ state of 8-chloroquinoline (15 MHz) is approximately the same as that observed for the $^3\pi\pi^*$ state of

DCB (22 MHz). However in 8-chloroquinoline the chlorine nuclear quadrupole constant is essentially unchanged upon excitation. In view of these observations it seems reasonable to interpret the change in $e^2qQ$ as arising from a bent C-Cl bond.

As we can see, ODMR offers many new possibilities for the measurement of the nuclear quadrupole coupling constants in excited triplet states.

The excellent sensitivity obtained with optical detection coupled with the accuracy of the measurement in zero field provides a new technique to obtain a detailed knowledge of the electron distribution and molecular geometry in excited states. We fully expect that these techniques will be applied to a variety of problems associated with organic molecules, inorganic molecules, semiconductors and various color centers in ionic solids. It has not been our intention to be exhaustive in this chapter, but rather to lay down a basic working knowledge of the theory and experimental methods to allow these techniques to be easily adapted to other questions and problems.

## References


1. S. P. McGlynn, T. Azumi and M. Kinoshito, Molecular Spectroscopy of the Triplet State (Prentice-Hall, Inc., 1969).
2. R. S. Becker, Theory and Interpretation of Fluorescence and Phosphorescence (Wiley Interscience, John Wiley & Sons, Inc., 1969).
3. S. K. Lower and M. A. El-Sayed, Chem. Rev., 66, 199 (1966).
4. M. S. DeGroot, I. A. M. Hesselmann and J. H. van der Waals, Mol. Phys. 12, 259 (1967).
5. G. N. Lewis and M. J. Kasha, J. Am. Chem. Soc. 66, 2100 (1944).
6. G. N. Lewis and M. J. Kasha, J. Am. Chem. Soc. 67, 994 (1945).
7. G. N. Lewis and M. Calvin, J. Am. Chem. Soc. 67, 1232 (1945).
8. G. N. Lewis, M. J. Kasha, and M. Calvin, J. Chem. Phys. 17, 804 (1949).
9. H. F. Hameka, Thesis, Leiden (1956).
10. C. A. Hutchison and B. W. Mangum, J. Chem. Phys. 29, 952 (1958).
11. C. A. Hutchison and B. W. Mangum, J. Chem. Phys. 34, 908 (1961).
12. Ph. Kottis and R. Lefebvre, J. Chem. Phys. 39, 393 (1963).
13. Ph. Kottis and R. Lefebvre, J. Chem. Phys. 41, 379 (1964).
14. S. Geschwind, G. E. Devlin, R. L. Cohen, and S. R. Chinn, Phys. Rev 137, AL087 (1965).
15. J. Brossel and A. Kastler, Compt. Rend. 229, 1213 (1949).
16. J. Brossel and F. Bitter, Phys. Rev. 86, 308 (1952).
17. M. Sharnoff, J. Chem. Phys. 46, 3263 (1967).
18. A. L. Kwiram, Chem. Phys. Letters 1, 272 (1967).
19. J. Schmidt, I. A. M. Hesselmann, M. S. DeGroot and J. H. van der Waals, Chem. Phys. Letters 1, 434 (1967).
20. J. Schmidt and J. H. van der Waals, Chem. Phys. Letters 2, 640 (1968).
21. R. W. Brandon, R. E. Gerkin and C. A. Hutchison, Jr., J. Chem. Phys. 41, 3717 (1968).
22. J. Schmidt and J. H. van der Waals, Chem. Phys. Letters 3, 546 (1969).
23. D. S. Tinti, M. A. El-Sayed, A. H. Maki and C. B. Harris, Chem. Phys. Letters 3, 343 (1969).
24. C. B. Harris, D. S. Tinti, M. A. El-Sayed and A. H. Maki, Chem. Phys. Letters 4, 409 (1969).

25. I. Y. Chan, J. Schmidt and J. H. van der Waals, Chem. Phys. Lett. 4, 269 (1969).

26. M. J. Buckley, C. B. Harris and A. H. Maki, Chem. Phys. Lett. 4, 591 (1970).

27. I. Y. Chan and J. H. van der Waals, Chem. Phys. Lett. 20, 157 (1973).

28. M. J. Buckley and C. B. Harris, Chem. Phys. Lett. 5, 205 (1970).

29. M. J. Buckley and C. B. Harris, J. Chem. Phys. 56, 137 (1972).

30. T. S. Kuan, D. S. Tinti and M. A. El-Sayed, Chem. Phys. Lett. 4, 507 (1970).

31. J. Schmidt, W. S. Veeman and J. H. van der Waals, Chem. Phys. Lett. 4, 341 (1969).

32. D. S. Tinti and M. A. El-Sayed, J. Chem. Phys. 54, 2529 (1971).

33. C. B. Harris and R. J. Hoover, J. Chem. Phys. 56, 2199 (1972).

34. C. J. Winscom and A. H. Maki, Chem. Phys. Lett. 12, 264 (1971).

35. D. A. Antheunis, J. Schmidt and J. H. van der Waals, Chem. Phys. Lett. 6, 255 (1970).

36. A. H. Francis, C. B. Harris and A. M. Nishimura, Chem. Phys. Lett. 14, 425 (1972).

37. C. R. Chen and M. A. El-Sayed, Chem. Phys. Lett. 16, 281 (1972).

38. G. Kothandaraman and D. S. Tinti, Chem. Phys. Lett. 19, 225 (1973).

39. M. J. Buckley, C. B. Harris and R. M. Panos, J. Am. Chem. Soc. 94, 3692 (1972).

40. A. I. Attia, B. H. Loo and A. H. Francis, Chem. Phys. Lett. 22, 537 (1973).

41. A. A. Gwaiz and M. A. El-Sayed, Chem. Phys. Let. 19, 11 (1973).

42. A. H. Francis and C. B. Harris, J. Chem. Phys. 57, 1050 (1972).

43. C. B. Harris, J. Chem. Phys. 54, 972 (1971).

44. J. Schmidt, W. G. van Dorp and J. H. van der Waals, Chem. Phys. Lett. 8, 345 (1971).

45. J. Schmidt, Chem. Phys. Lett. 14, 411 (1972).

46. W. G. Breiland, C. B. Harris and A. Pines, Phys. Rev. Lett. 30, 158 (1973).

47. C. B. Harris, R. L. Schlupp and H. Schuch, Phys. Rev. Lett. 30, 1019 (1973).

48. C. A. van't Hoff, J. Schmidt, P. J. F. Verbeck and J. H. van der Waals, Chem. Phys. Lett. 21, 437 (1973).

49. H. C. Brenner, J. C. Brock and C. B. Harris, J. Chem. Phys. 60, 4448 (1974).

50. M. J. Buckley and A. H. Francis, Chem. Phys. Lett. 23, 582 (1973).

51. S. J. Hunter, H. Parker and A. H. Francis, J. Chem. Phys. 61, 1390 (1974).

52. A. H. Zewail and C. B. Harris, Chem. Phys. Lett. 28, 8 (1974).

53. A. H. Francis and C. B. Harris, Chem. Phys. Lett. 9, 181; 188 (1971).

54. C. B. Harris, M. Glasbeek and E. B. Hensley, Phys. Rev. Lett. 33, 537 (1974).

55. M. A. El-Sayed, J. Chem. Phys. 54, 680 (1971).

56. M. A. El-Sayed, D. S. Tinti and E. M. Yee, J. Chem. Phys. 51, 5721 (1969); M. A. El-Sayed, D. S. Tinti and O. V. Owens, Chem. Phys. Lett. 3, 339 (1969); M. A. El-Sayed, J. Chem. Phys. 52, 6438 (1970); M. A. El-Sayed and O. F. Kalman, J. Chem. Phys. 52, 4903 (1970).

57. H. F. Hameka, in The Triplet State (proc. Intl. Symposium on the Triplet State, 1967), Cambridge Univ. Press (1967), p. 25.

58. E. Gilmore, G. Gibson and D. McClure, J. Chem. Phys. 20, 829 (1952); 23, 399 (1955).

59. M. S. de Groot and J. H. van der Waals, Mol. Phys. 6, 545 (1963).

60. M. J. Buckley and C. B. Harris, unpublished results.

61. M. Tinkham and M. W. P. Strandberg, Phys. Rev. 97, 937 (1955); M. Gouterman and W. Moffitt, J. Chem. Phys. 30, 1107 (1959).

62. A. Carrington and A. D. McLachlan, Introduction to Magnetic Resonance, Harper and Row (1967), p. 117.

63. T. P. Das and E. L. Hahn, Nuclear Quadrupole Resonance Spectroscopy, Academic Press, New York (1958); M. H. Cohen and F. Reif, Solid State Physics, Vol. V, Academic Press, New York (1957); E. A. C. Lucken, Nuclear Quadrupole Coupling Constants, Academic Press, New York (1969).

64. J. S. Vincent and A. H. Maki, J. Chem. Phys. 42, 865 (1965).

65. R. H. Webb, Rev. Sci. Instr. 33, 732 (1962).

66. M. Kasha, J. Opt. Sci. Am. 38, 929 (1948).

67. D. Owens, M. A. El-Sayed and S. Ziegler, J. Chem. Phys. 52, 4315 (1970).

68. C. A. Hutchison Jr., J. V. Nicholas and G. W. Scott, J. Chem. Phys. 53, 1906 (1970).

69. Y. Gondo and A. H. Maki, J. Chem. Phys. 50, 3270 (1969).

70. D. Pooley and D. H. Wiffen, Spectrochimica Acta 18, 291 (1962).

71. H. R. Falle, G. R. Luckhurst, A. Horsfield and M. Ballester, J. Chem. Phys. 50, 258 (1969).

72. J. Schmidt, W. S. Veeman and J. H. van der Waals, Chem. Phys. Lett. 4, 341 (1969).

73. E. A. C. Lucken, Trans. Faraday Soc. 57, 729 (1961).

74. E. Schempp and P. J. Bray, J. Chem. Phys. 46, 1186 (1967).

75. S. L. Segal, R. G. Barnes and P. J. Bray, J. Chem. Phys. 25, 1286 (1956).

76. M. Dewar and E. Lucken, J. Chem. Soc. (London), 2653 (1958).

77. M. S. De Groot, I. A. M. Hesselman and J. H. van der Waals, Mol. Phys. 16, 45 (1969).

78. D. S. Tinti, G. Kothandaraman and C. B. Harris, J. Chem. Phys. 59, 190 (1973).

79. N. Hirota, C. A. Hutchison Jr., and P. Palmer, J. Chem. Phys. 40, 3717 (1964).

80. P. J. Bray, R. G. Barnes and R. Bersohn, J. Chem. Phys. 25, 813 (1956).

81. H. Bayer, Z. Physik 130, 227 (1951).

82. R. Bersohn, J. Chem. Phys. 22, 2078 (1954).

TABLE 1

Techniques of Optical Detection of ESR

| | Excitation Light | Optical Spectrometer | Microwave Modulation | Advantages |
|---|---|---|---|---|
| 1) | C.W. | No | No | measure absolute change in total emission |
| 2) | C.W. | Yes | No | Measure absolute change in emission of particular vibronic bands |
| 3) | Chopped | Optional | No | Improvement in S/N over Methods 1 and 2 by narrow band phase sensitive detection of the phosphorescence |
| 4) | C.W. | Optional | A.M. | detect only the change in emission from either the total emission or a particular vibronic band |
| 5) | C.W. | Optional | F.M. | detect the derivative of the spectrum, helpful in resolving spectra |
| 6) | C.W. | Sweep | A.M. | detect only the emission from 2 of the 3 sublevels while sweeping the optical spectrum |
| 7) | Sweep | Yes | A.M. | useful in studying the pathways of intersystem crossing |

TABLE 2

Spin Hamiltonian parameters and triplet lifetimes of the $^3\pi\pi^*$ states of 8-chloroquinoline and quinoline.

| | 8-chloroquinoline in durene (1.3°K) | quinoline in durene (1.35°K)[a] |
|---|---|---|
| Y (MHz) | 1414.5 | 1528.5 |
| Z (MHz) | 555.5 | 528.0 |
| X (MHz) | -1970.0 | -2056.5 |
| D[b] (MHz) | 2399.5 | 2556.75 |
| E[b] (MHz) | -429.5 | -500.25 |
| $A_{xx}^{N}$ (MHz) | 19.5 | 22.[c] |
| $A_{xx}^{Cl}$ (MHz) | 15. | --- |
| $e^2qQ(^{14}N)$[d] (MHz) | 4.27 | ~ 4.0[e] |
| $e^2qQ(^{35}Cl)$ (MHz) | -68.4 | --- |
| $\tau_x$ (sec) | ≥1 | 5.0 |
| $\tau_y$ (sec) | 0.11 | 0.32 |
| $\tau_z$ (sec) | ≥1 | 2.7 |

[a] data from reference 72

[b] with the definitions D = - 3/2X and E = - 1/2(Y-Z)

[c] data from reference 64

[d] with the assumptions $e^2qQ(^{14}N) = 4/3(y-z)$

[e] data from reference 26

TABLE 3 Measured and calculated ESR transitions of the $^3\pi\pi^*$ state of of 8-chloroquinoline

| | Measured frequency (±0.5 MHz) | Calculated frequency | Classification |
|---|---|---|---|
| a) $\tau_x \rightarrow \tau_y$ | | | |
| | 3422.8 | 3422.7 | E |
| | 3419.5 | 3419.5 | C |
| | 3416.5 | 3416.5 | E |
| | 3415.3 | 3415.3 | F |
| | 3412.0 | 3412.1 | D |
| | 3409.3 | 3409.1 | F |
| | 3388.9 | 3388.3 | B |
| | 3385.9 | 3385.1 | A |
| | 3382.7 | 3382.2 | B |
| | 3361.2 | 3361.1 | F |
| | 3358.1 | 3358.0 | D |
| | 3354.5 | 3355.2 | F |
| | 3353.9 | 3353.9 | E |
| | 3350.9 | 3350.8 | C |
| | 3347.6 | 3348.0 | E |
| b) $\tau_x \rightarrow \tau_z$ | | | |
| | 2562.3 | 2561.9 | E |
| | 2559.3 | 2558.9 | C |
| | 2555.8 | 2555.7 2554.8 | E,F |
| | 2552.3 | 2551.8 | D |
| | 2548.9 | 2548.6 | F |
| | 2525.5 | 2524.9 | A |
| | 2501.7 | 2500.9 | F |
| | 2498.0 | 2498.1 | D |
| | 2494.4 | 2493.6 2495.0 | E,F |
| | 2491.0 | 2490.8 | C |
| | 2487.9 | 2487.7 | E |
| c) $\tau_z \rightarrow \tau_y$ | | | |
| | 898.1 | 897.9 | E |
| | 895.6 | 894.7 | C |
| | 891.7 | 891.6 | E |
| | 890.7 | 890.4 | F |
| | 888.2 | 887.3 | D |
| | 884.3 | 884.2 | F |
| | 863.8 | 864.1 | B |
| | 860.1 | 860.2 | A |
| | 857.3 | 857.4 | B |
| | 836.4 | 836.4 | F |
| | 833.5 | 833.4 | D |
| | 830.8 | 830.3 | F |
| | 829.8 | 829.4 | E |
| | 826.5 | 826.0 | C |
| | 822.9 | 823.2 | E |

TABLE 4

ESR Transitions in Paradichlorobenzene

| Transition Type | Simultaneous Transitions | Molecular Species |
|---|---|---|
| A | Electron Spin | I, II, III |
| B | Electron and $^{35}Cl$ Spins | I, II |
| C | Electron and $^{37}Cl$ Spins | II, III |
| D | Electron, $^{35}Cl$ and $^{35}Cl$ Spins | I |
| E | Electron, $^{35}Cl$ and $^{37}Cl$ Spins | II |
| F | Electron, $^{37}Cl$ and $^{37}Cl$ Spins | III |

TABLE 5

Zero-Field Splitting Parameters (MHz)

| | Paradichlorobenzene * | | Benzene† -$h_4$ |
|---|---|---|---|
| | X Trap (1.3°K) | Y Trap (4.2°K) | In Benzene-$d_6$ (1.95°K) |
| X | -2988.75 | -2967.7 | -3159.8 |
| Z | 616.07 | 654.4 | 1769.4 |
| Y | 2372.68 | 2313.4 | 1385.0 |
| $D^{\ddagger}$ | 4483.13 | 4451.6 | 4739.7 |
| $E^{\ddagger}$ | -878.31 | -829.5 | +192.2 |
| $D^{*}$ | 4733.8 | 4677.7 | 4793.2 |
| $e^2qQ$ | -64.5 | - | - |
| $A_{xx}(^{35}Cl)$ | 22 | - | - |

‡ In order to be consistent with the standard ESR definitions we have defined

$$D = -3/2\ X \quad \text{and} \quad E = 1/2\ (Z-Y)$$

† Data from reference 77 expressed in our axis system.

* Phosphorescence origin: X trap (27868 $cm^{-1}$) and Y trap (27807 $cm^{-1}$).

TABLE 6

Measured and Calculated ESR Transitions of the $^3\pi\pi^*$ State of Paradichlorobenzene (X Trap)

| | Measured Frequency (MHz) | σ | Calculated Frequency | Classification |
|---|---|---|---|---|
| a) $\tau_x \rightarrow \tau_y$ | | | | |
| | 5426.7 | 1.0* | 5426.91 | D |
| | 5419.6 | 1.0* | 5419.56 | E |
| | 5394.56 | 0.41 | 5394.62 | B |
| | 5387.86 | 0.41 | 5387.79 | C |
| | 5368.73 | 0.64 | 5368.89 | E |
| | 5362.20 | 0.34 | 5362.14 | A |
| | 5355.13 | 0.25 | 5355.12 | E |
| | 5336.67 | 0.24 | 5366.50 | C |
| | 5329.74 | 0.28 | 5329.75 | B |
| | 5303.8 | 1.0* | 5304.11 | E |
| | 5296.5 | 1.0* | 5297.35 | D |
| b) $\tau_x \rightarrow \tau_z$ | 3636.03 | .07 | 3636.13 | B |
| | 3629.65 | .18 | 3629.56 | C |
| | 3611.18 | .24 | 3611.04 | E |
| | 3604.19 | .25 | 3604.10 | A |
| | 3597.69 | .31 | 3597.43 | E |
| | 3578.90 | .22 | 3578.89 | C |
| | 3571.88 | .34 | 3571.99 | B |
| c) $\tau_z \rightarrow \tau_y$ | 1791.1 | 1.5 | 1791.13 | B |
| | 1758.2 | 1.0 | 1758.05 | A |
| | 1724.5 | 1.5 | 1726.55 | B |

* Estimated value of the standard deviation σ

TABLE 7

Measured and Calculated Chlorine ENDOR Transitions of the $^3\pi\pi^*$ State of Paradichlorobenzene (X Trap)

| Measured Frequency in MHz (±.05) | Calculated Frequency in MHz (range) |
|---|---|
| $\tau_x \rightarrow \tau_y$ Manifold | |
| $^{35}Cl$ 32.06; 32.96 | 31.56 - 33.03 |
| $^{37}Cl$ 25.12; 26.00 | 24.94 - 26.09 |
| $\tau_x \rightarrow \tau_z$ Manifold | |
| $^{35}Cl$ 31.75; 33.13 | 31.53 - 32.94 |
| $^{37}Cl$ 24.94; 26.19 | 24.79 - 25.90 |

TABLE 8

Contributions to the Chlorine Nuclear Quadrupole Coupling Constant

| Chlorine Orbital | No. of Holes | Contribution to $V_{xx}$ | $V_{yy}$ | $V_{zz}$ |
|---|---|---|---|---|
| $P_x$ | $\delta$ | $\delta q$ | $-\delta q/2$ | $-\delta q/2$ |
| $P_z$ | $\sigma$ | $-\sigma q/2$ | $-\sigma q/2$ | $\sigma q$ |

Total Contribution

$$V_{xx} = (\delta - \sigma/2)q$$

$$V_{yy} = -1/2(\delta + \sigma)q$$

$$V_{zz} = (\sigma - \delta/2)q$$

## Figure Captions

Fig. 1 Relaxation pathways and rate constants for the triplet state.

Fig. 2 Relaxation pathways and rate constants considering only two of the three triplet levels (see text).

Fig. 3 Population change predicted for ESR ($b \leftrightarrow d$) and ENDOR ($a \leftrightarrow b$) transitions.

Fig. 4 Energy level diagram for the triplet and one $I = 1$ nuclear spin considering only the $A_{xx}$ hyperfine component.

Fig. 5 ODMR spectra predicted for the energy level diagram shown in Fig. 4.

Fig. 6 Energy level diagram for the triplet and one $I = 3/2$ nuclear spin considering only the $A_{xx}$ hyperfine component.

Fig. 7 ODMR spectra predicted for the energy level diagram shown in Fig. 6.

Fig. 8 Energy level diagram for the triplet and one $I = 3/2$ nuclear spin considering only the $A_{zz}$ hyperfine component.

Fig. 9 ODMR spectra predicted for the energy level diagram shown in Fig. 8.

Fig. 10 Experimental arrangement used in performing ODMR experiments in zero field with amplitude modulation of the microwave field.

Fig. 11 Experimental arrangement for optically detected ENDOR in zero magnetic field. An enlarged view of the sample and ENDOR coil schematic is shown on the left.

Fig. 12 The $\tau_x \rightarrow \tau_y$, $\tau_x \rightarrow \tau_z$ and $\tau_z \rightarrow \tau_y$ optically detected ESR transitions in 8-chloroquinoline using relatively high microwave power. The $\tau_x \rightarrow \tau_z$ transition was obtained by performing an EEDOR experiment.

Fig. 13 Optically detected $^{35}Cl$ ENDOR observed while saturating the $\tau_y \rightarrow \tau_z$ multiplet.

Fig. 14 Energy level diagram for 8-chloroquinoline.

Fig. 15 ODMR of the $\tau_x \rightarrow \tau_y$ multiplet of paradichlorobenzene.

Fig. 16 $^{35}Cl$ ENDOR resonance associated with the $\tau_x \rightarrow \tau_y$ and $\tau_x \rightarrow \tau_z$ electron spin transitions.

Fig. 17 $^{35}Cl$ ENDOR pumping of the $\tau_x \rightarrow \tau_y$ multiplet.

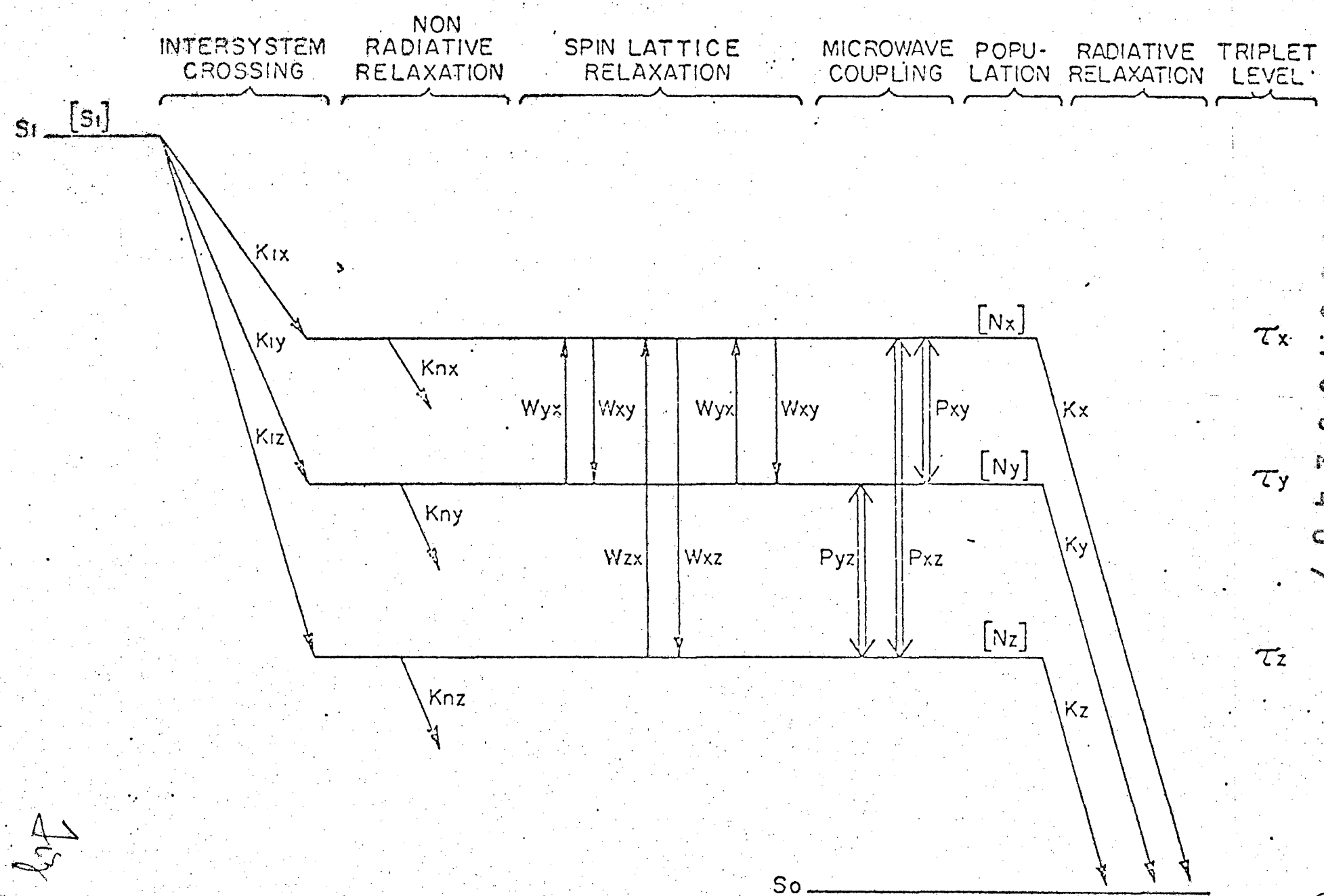
INTERSYSTEM CROSSING
NON RADIATIVE RELAXATION
SPIN LATTICE RELAXATION
MICROWAVE COUPLING
POPU- LATION
RADIATIVE RELAXATION
TRIPLET LEVEL
S1
[S1]
K1x
K1y
K1z
Knx
Kny
Knz
[Nx]
[Ny]
[Nz]
Wyx
Wxy
Wyx
Wxy
Pxy
Wzx
Wxz
Pyz
Pxz
Kx
Ky
Kz
So
τx
τy
τz

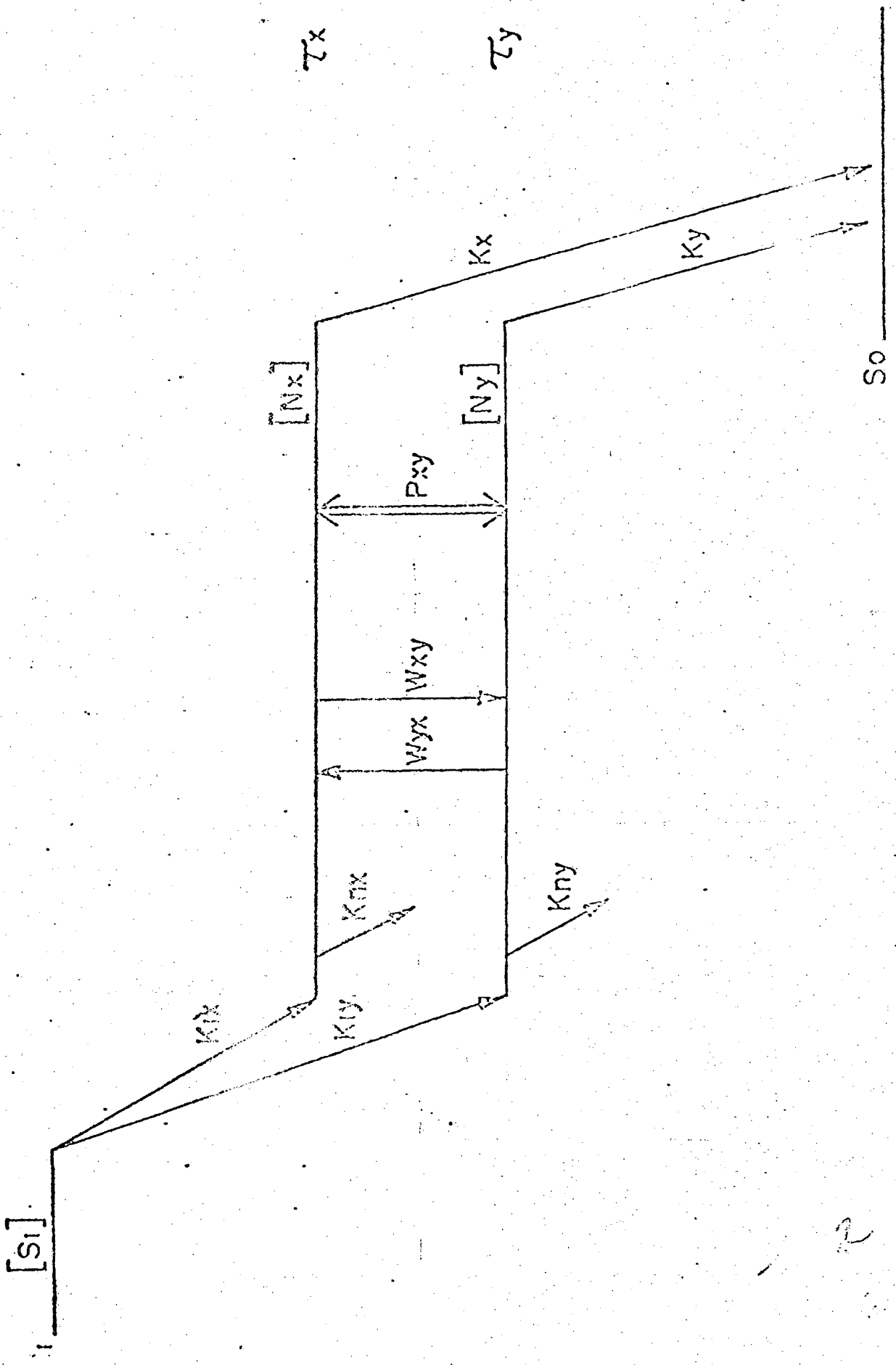
τx
τy
Kx
Ky
So
[Nx]
[Ny]
Pxy
Wxy
Wyx
Kmx
Kny
Kmy
Kx
Ky
[Si]

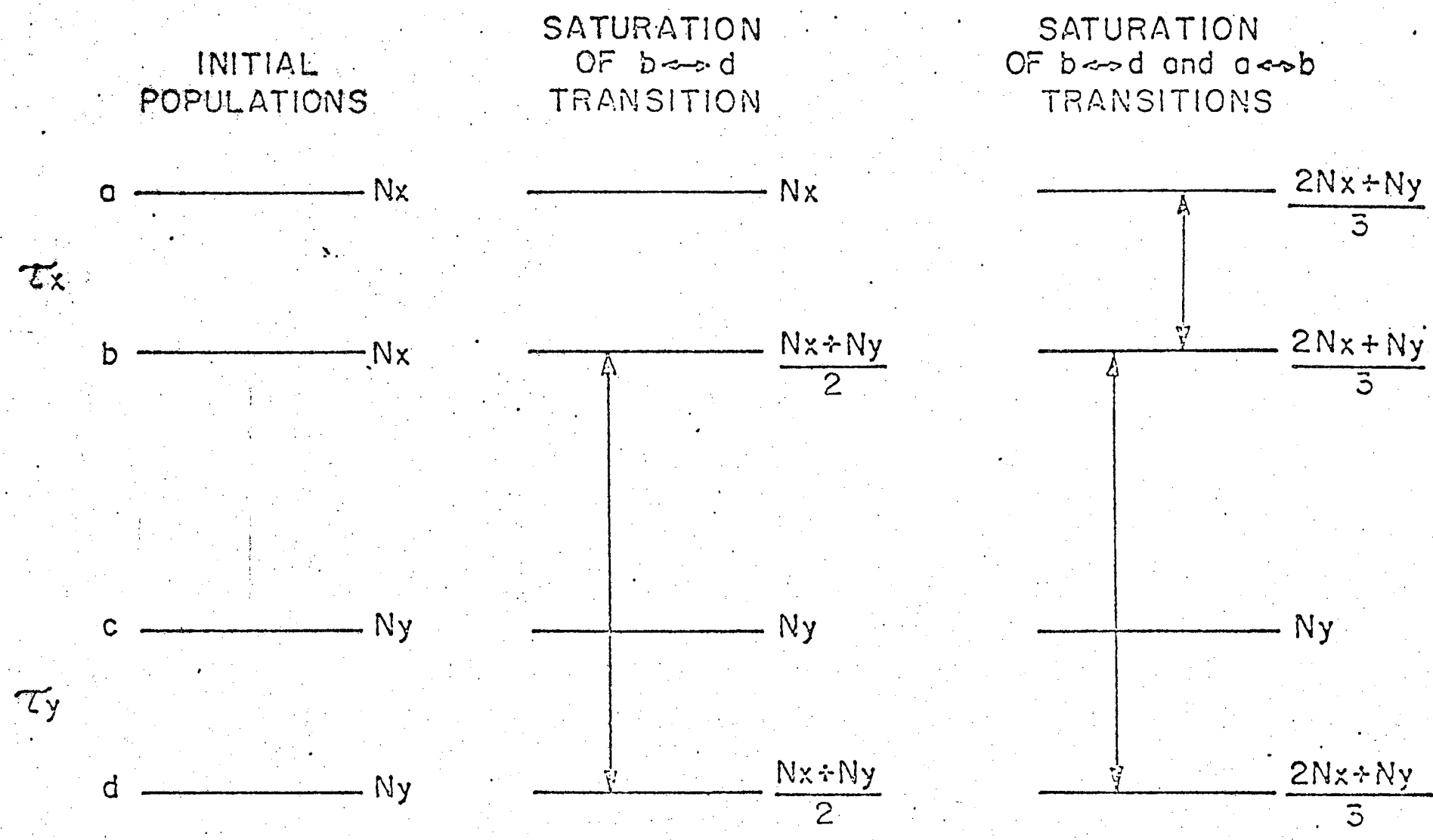
INITIAL POPULATIONS
SATURATION OF b⇔d TRANSITION
SATURATION OF b⇔d and a⇔b TRANSITIONS
a
b
c
d
Nx
Nx
Ny
Ny
τx
τy
Nx
Nx÷Ny / 2
Ny
Nx÷Ny / 2
2Nx÷Ny / 3
2Nx+Ny / 3
Ny
2Nx÷Ny / 3

Fig 3

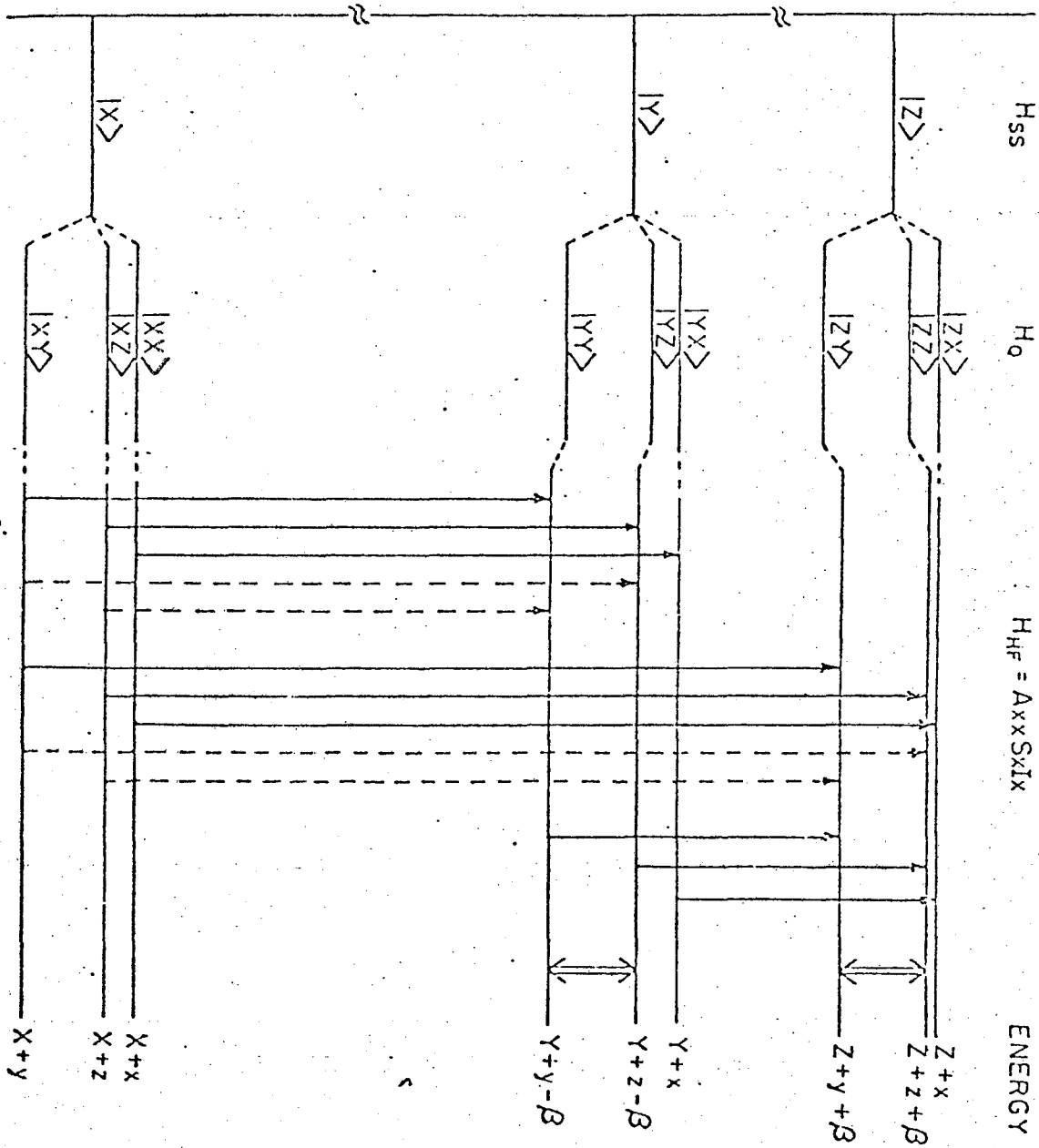
$H_{ss}$
$H_0$
$H_{HF} = A_{xx} S_x I_x$
ENERGY
|X>
|Y>
|Z>
|XY>
|XZ>
|XX>
|YY>
|YZ>
|YX>
|ZY>
|ZZ>
|ZX>
X+y
X+z
X+x
Y+y-β
Y+z-β
Y+x
Z+y+β
Z+z+β
Z+x

Fig 4

a) $\tau_x \rightarrow \tau_z$

$\nu_o = Z - X$

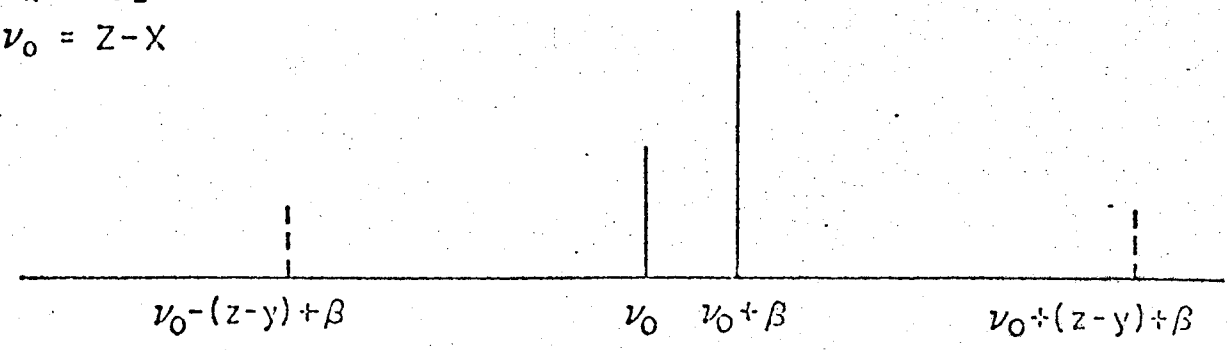


b) $\tau_x \rightarrow \tau_y$

$\nu_o = Y - X$

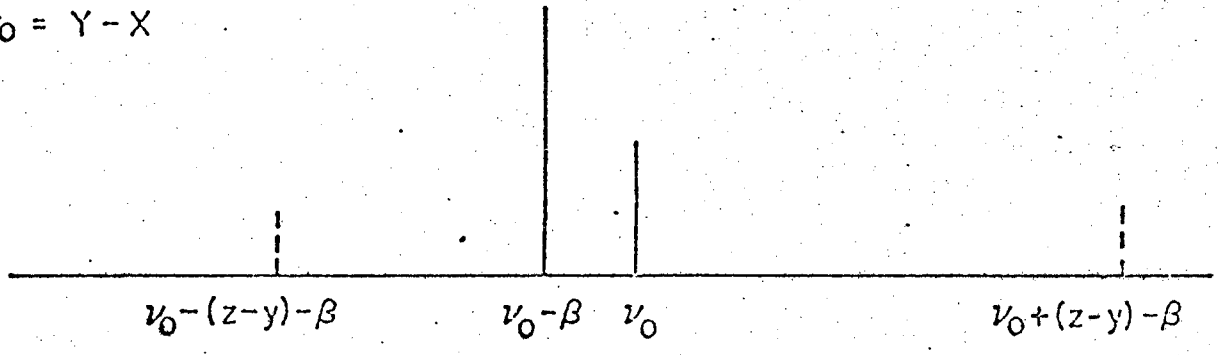


c) $\tau_y \rightarrow \tau_z$

$\nu_o = Z - Y$

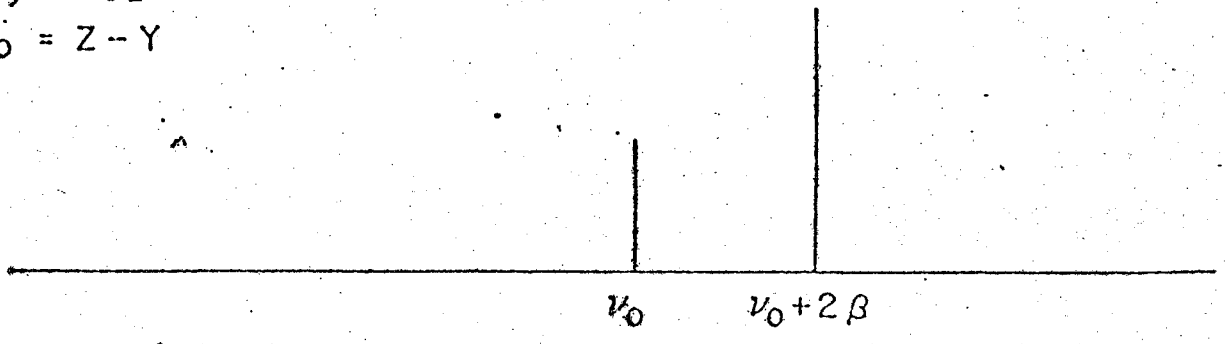

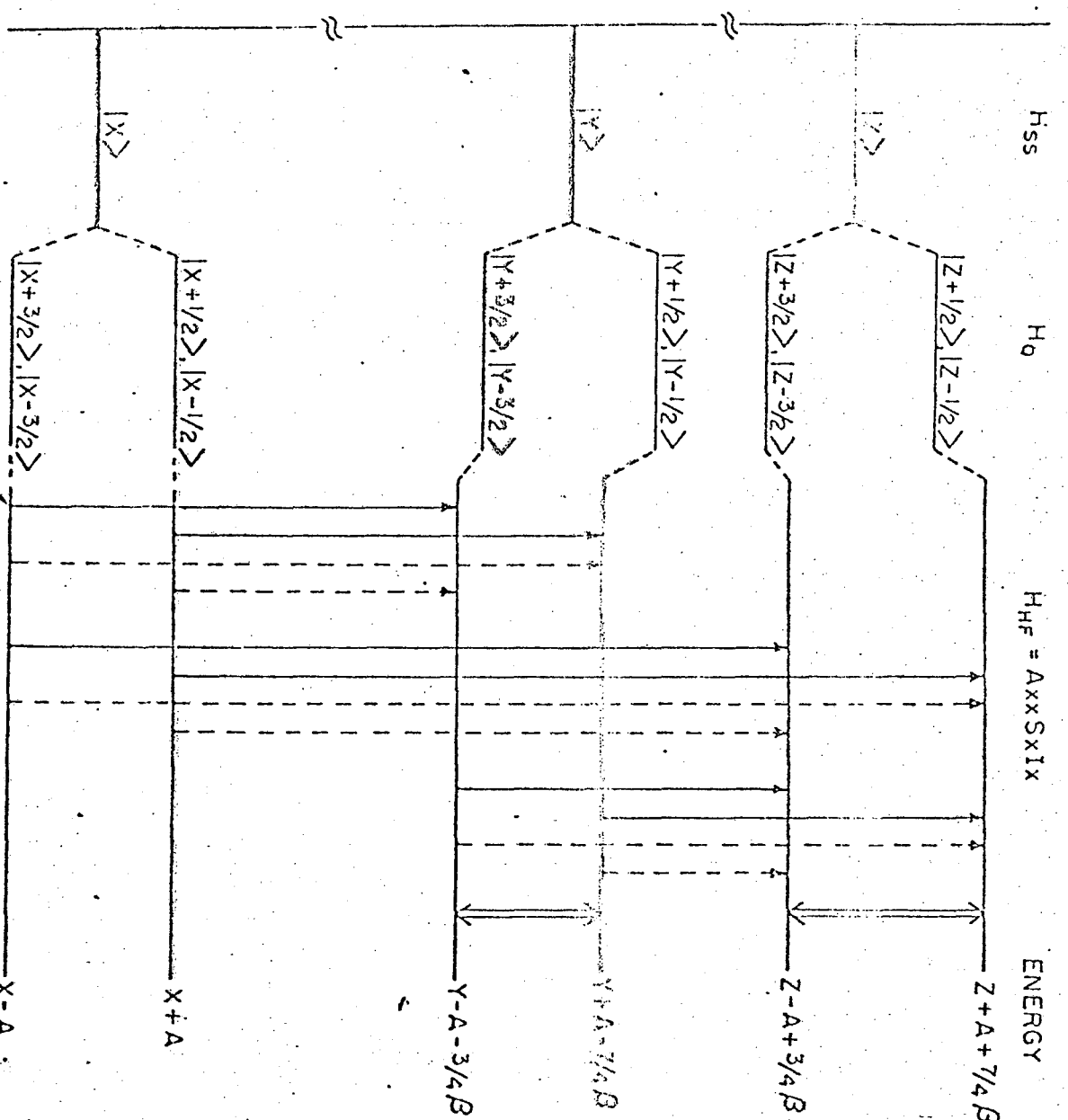
Hss
H0
HHF = AxxSxIx
ENERGY
|Z+1/2>,|Z-1/2>
|Z+3/2>,|Z-3/2>
|Y+1/2>,|Y-1/2>
|Y+3/2>,|Y-3/2>
|X+1/2>,|X-1/2>
|X+3/2>,|X-3/2>
Z+A+7/4β
Z-A+3/4β
Y-A-3/4β
X+A
X-A

a) $\tau_x \rightarrow \tau_z$
$\nu_0 = Z - X$

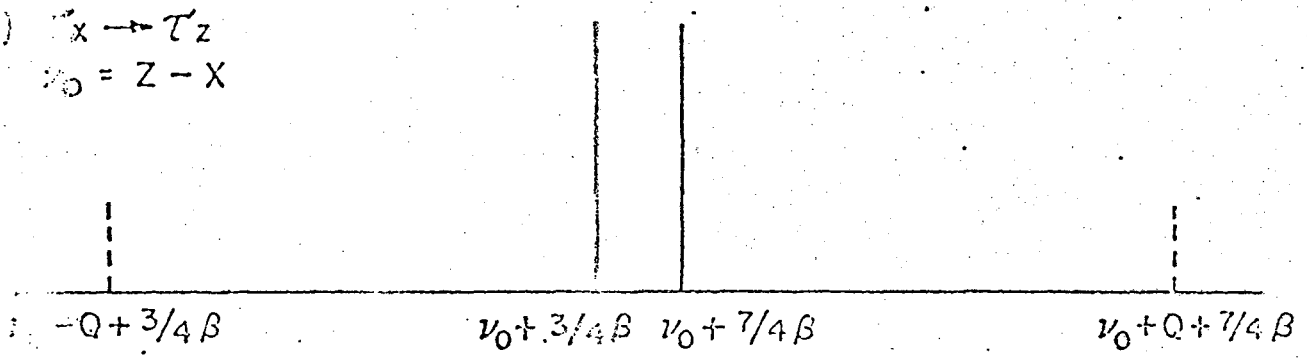


b) $\tau_y \rightarrow \tau_y$
$\nu_0 = Y - X$

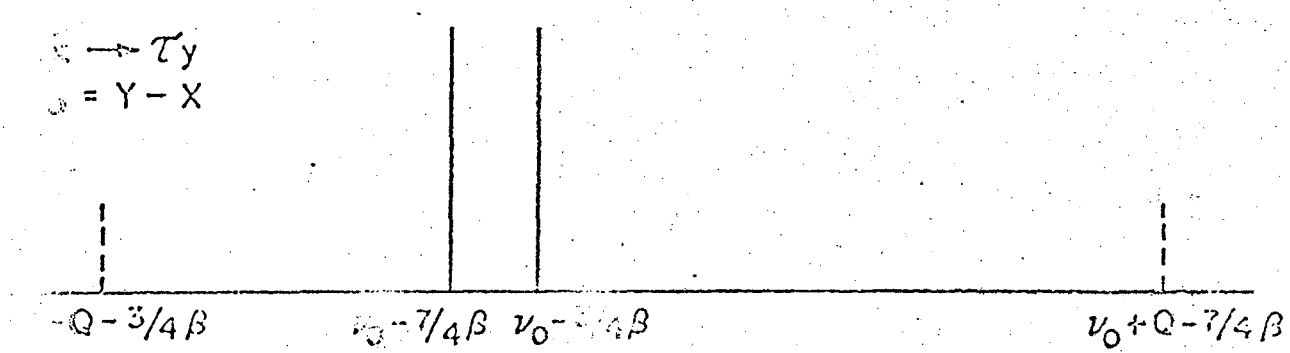


c) $\tau_z \rightarrow \tau_z$
$= Z - Y$

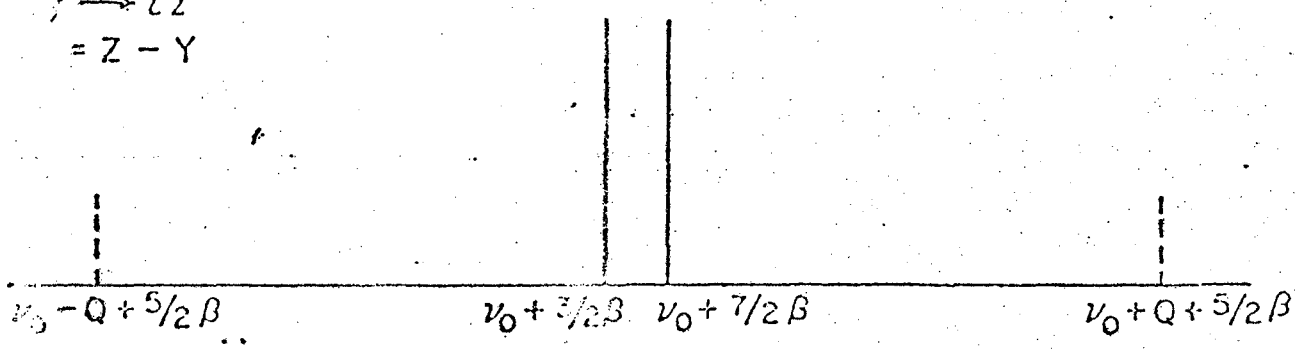


fig 1

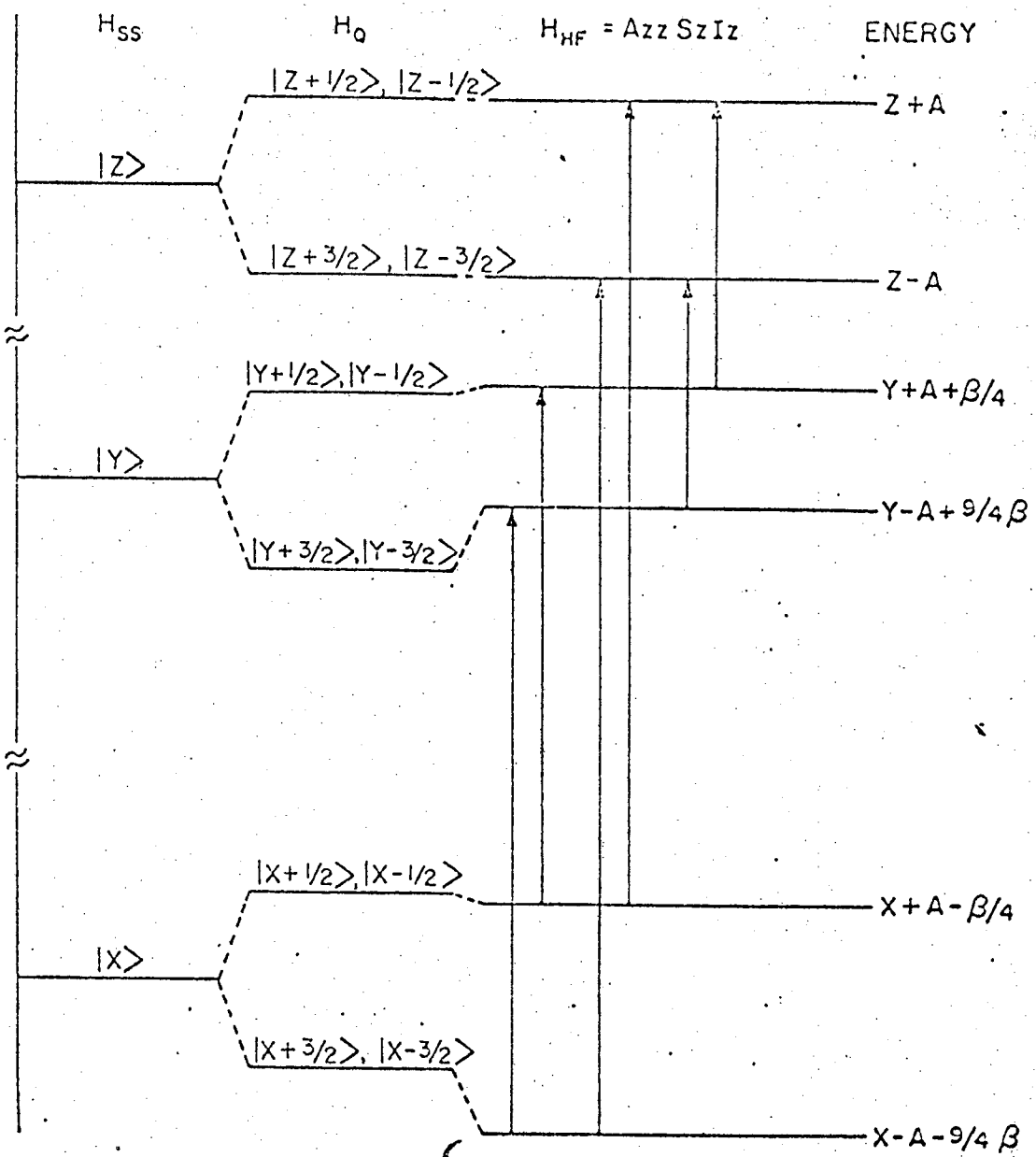
$H_{SS}$
$H_Q$
$H_{HF} = Azz\ Sz\ Iz$
ENERGY
$|Z+1/2\rangle, |Z-1/2\rangle$
$Z+A$
$|Z\rangle$
$|Z+3/2\rangle, |Z-3/2\rangle$
$Z-A$
$|Y+1/2\rangle, |Y-1/2\rangle$
$Y+A+\beta/4$
$|Y\rangle$
$Y-A+9/4\beta$
$|Y+3/2\rangle, |Y-3/2\rangle$
$|X+1/2\rangle, |X-1/2\rangle$
$X+A-\beta/4$
$|X\rangle$
$|X+3/2\rangle, |X-3/2\rangle$
$X-A-9/4\beta$

a) $\tau_x \rightarrow \tau_z$
$\nu_0 = Z - X$

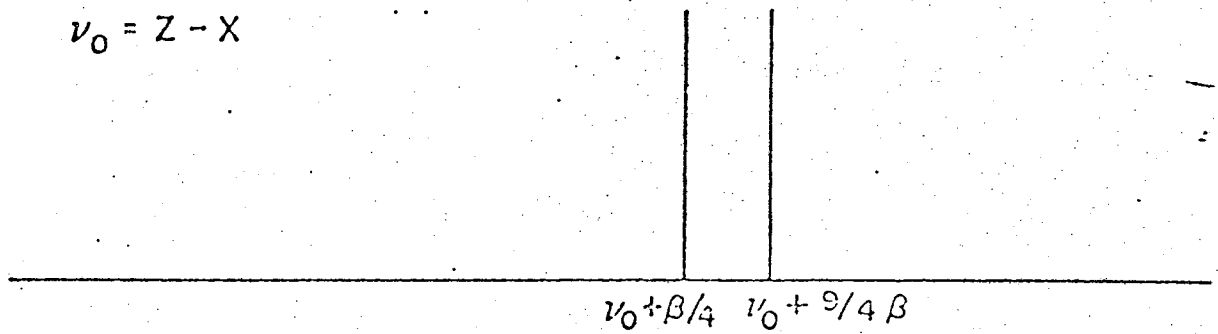


b) $\tau_x \rightarrow \tau_y$
$\nu_0 = Y - X$

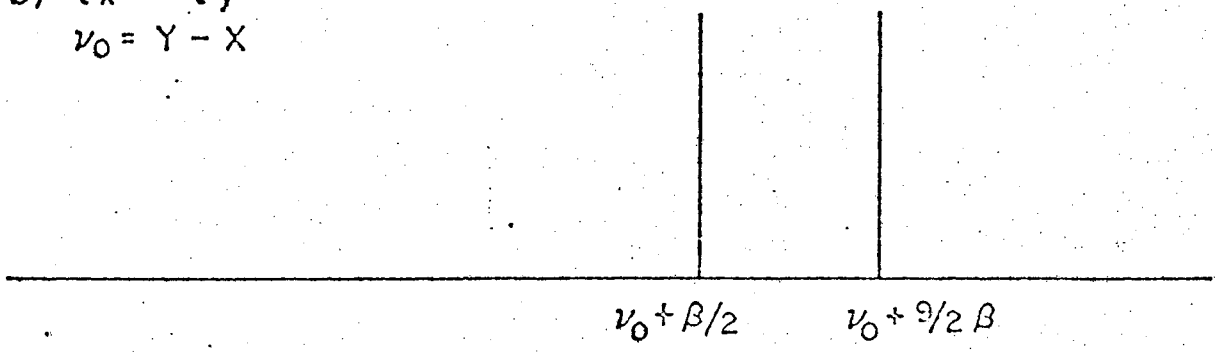


c) $\tau_y \rightarrow \tau_z$
$\nu_0 = Z - Y$

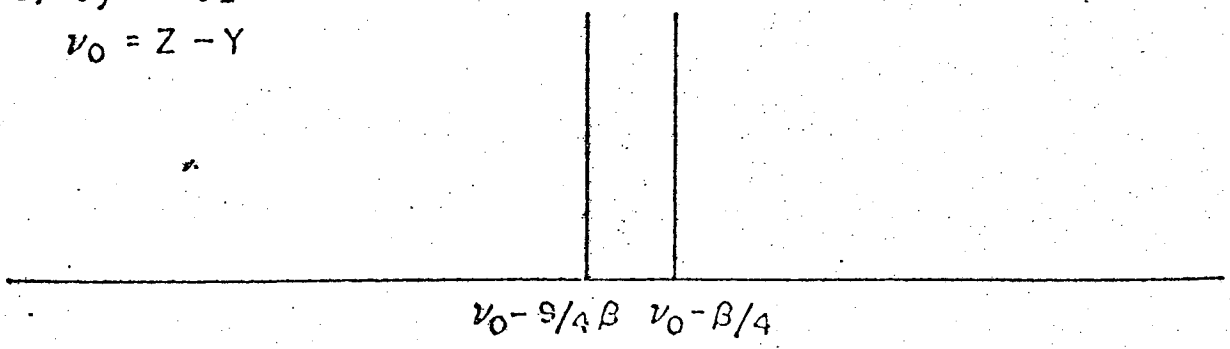


Fig 9

# ESR EXPERIMENT

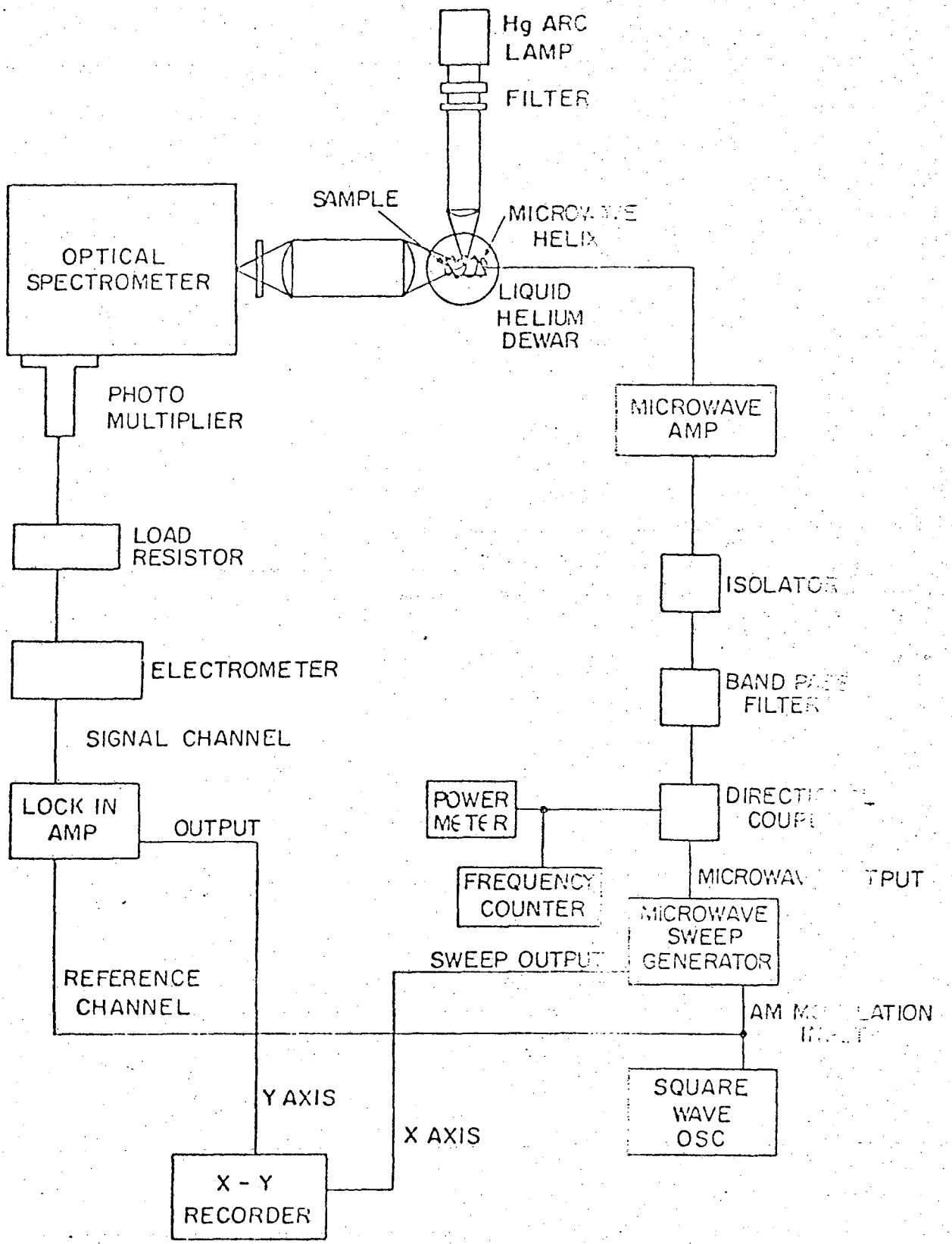

## ENDOR EXPERIMENT

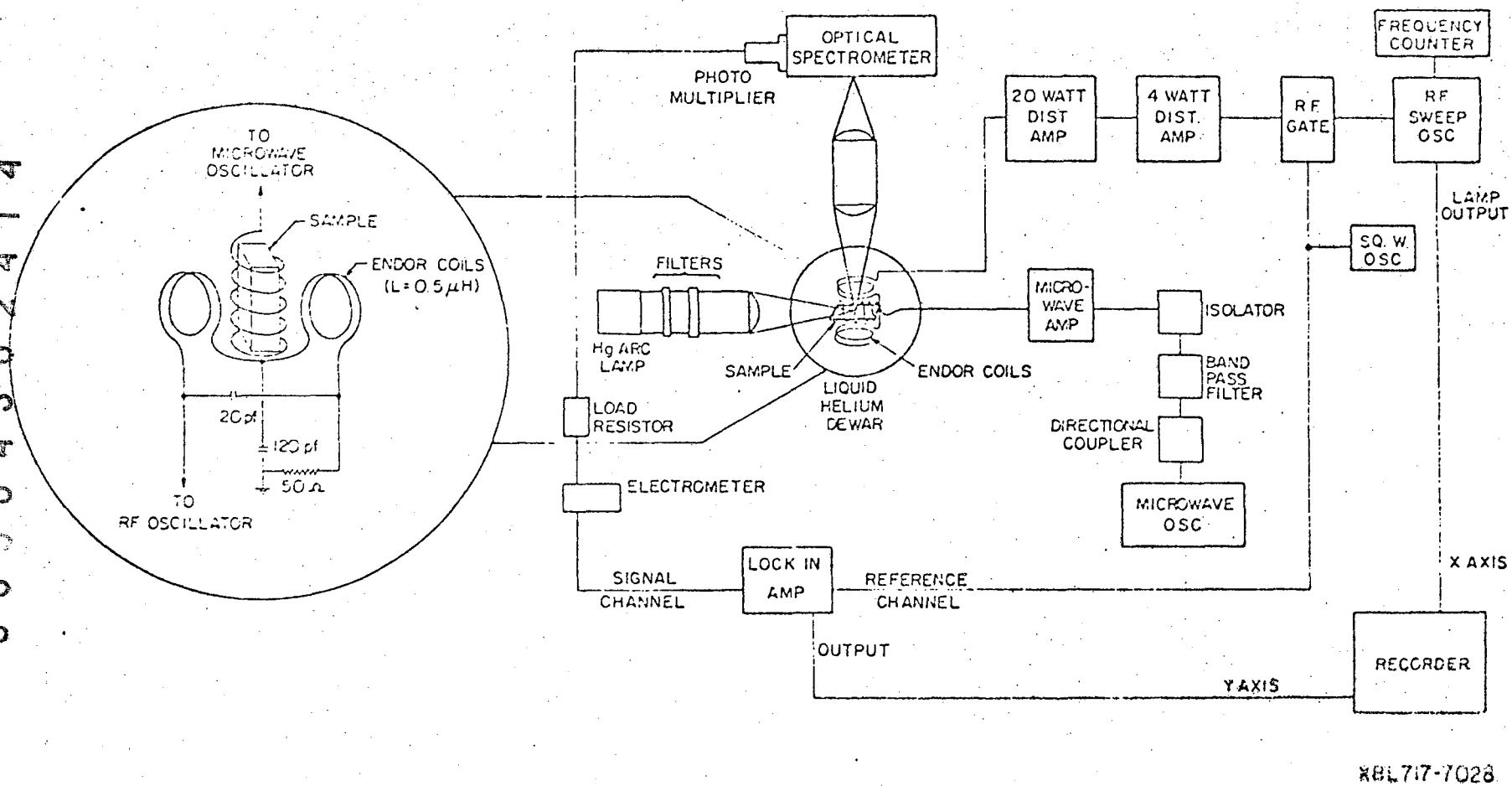


XBL717-7028

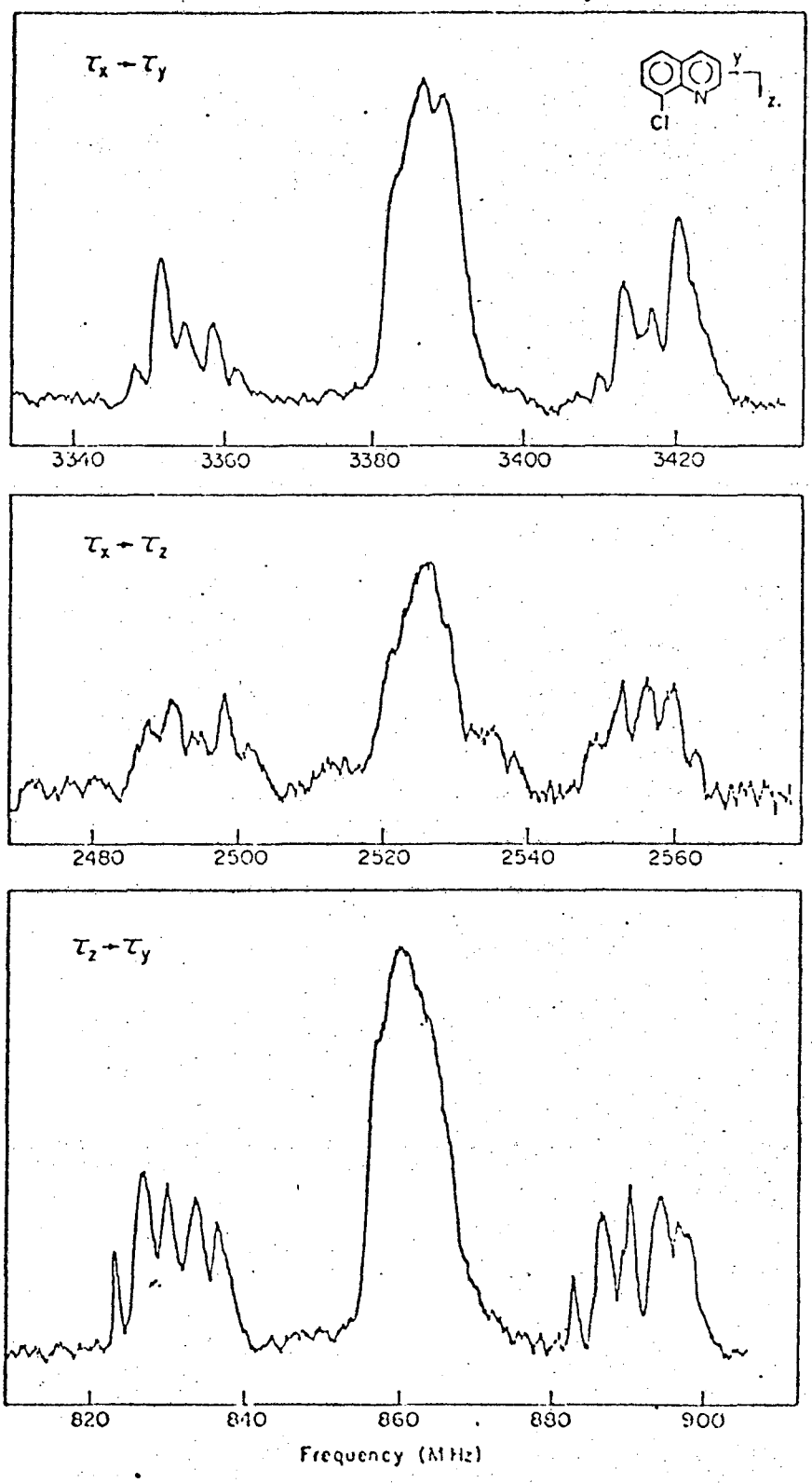


XBL716-6866

fig 1 fig 1

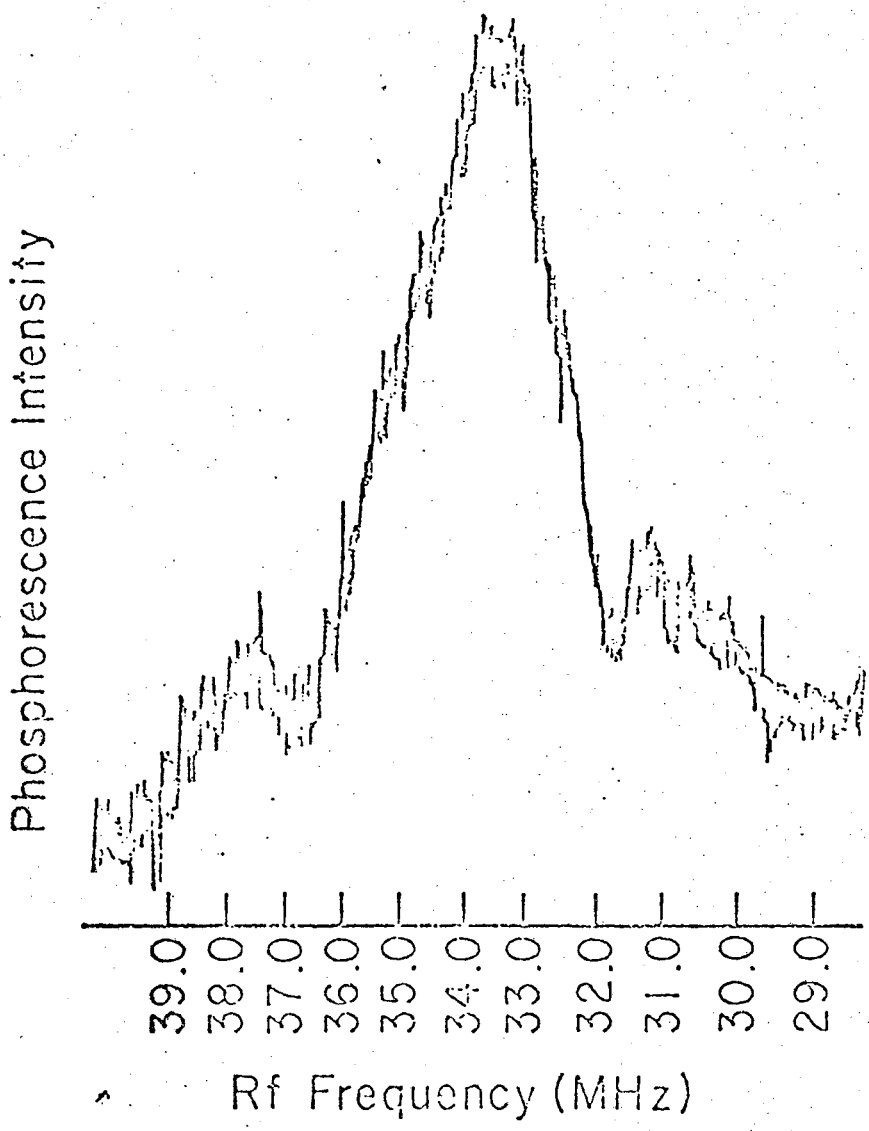
Phosphorescence Intensity
39.0
38.0
37.0
36.0
35.0
34.0
33.0
32.0
31.0
30.0
29.0
Rf Frequency (MHz)

Fig 13

Fig 13

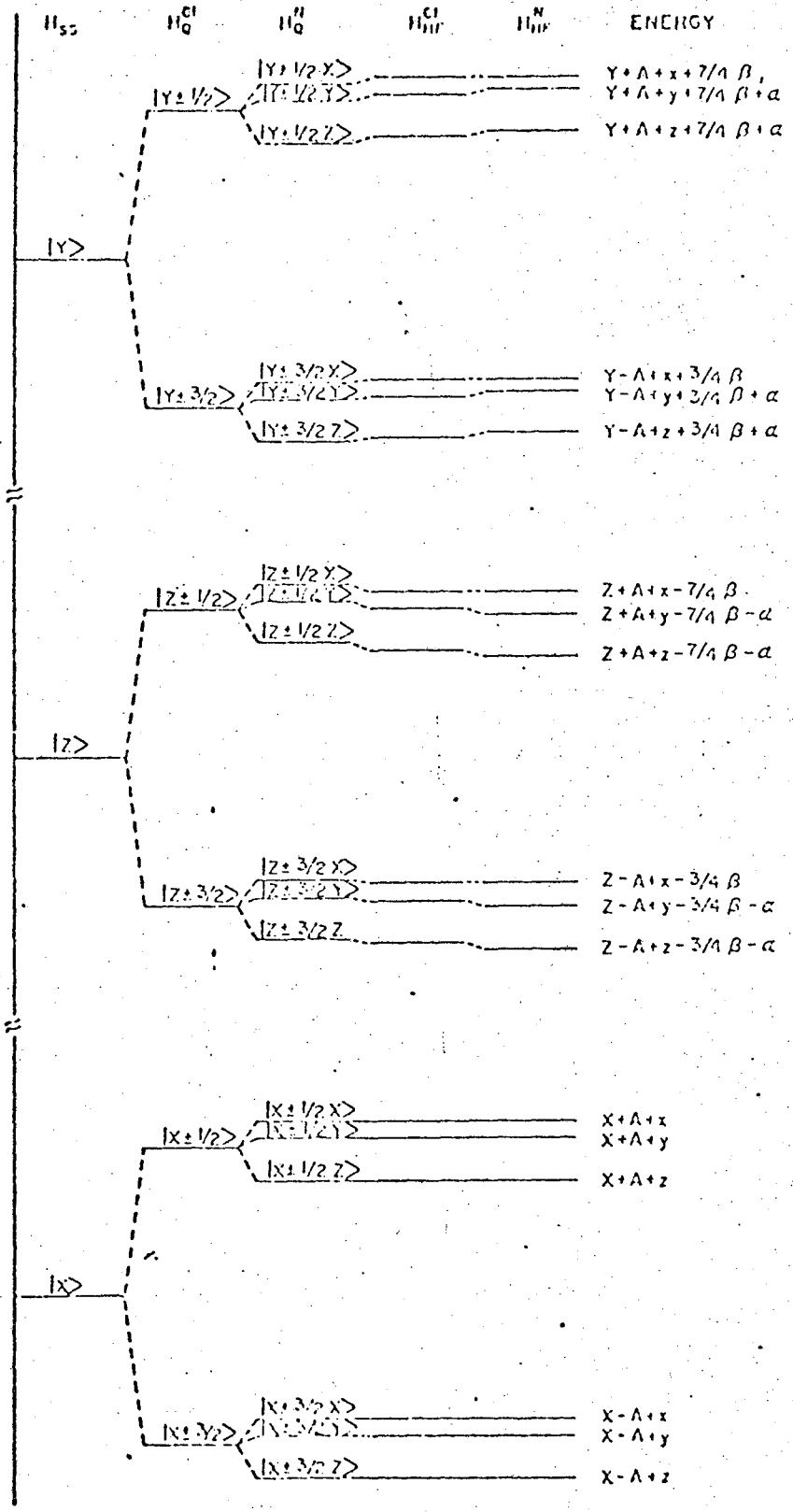


XBL716-6865

Fig 14

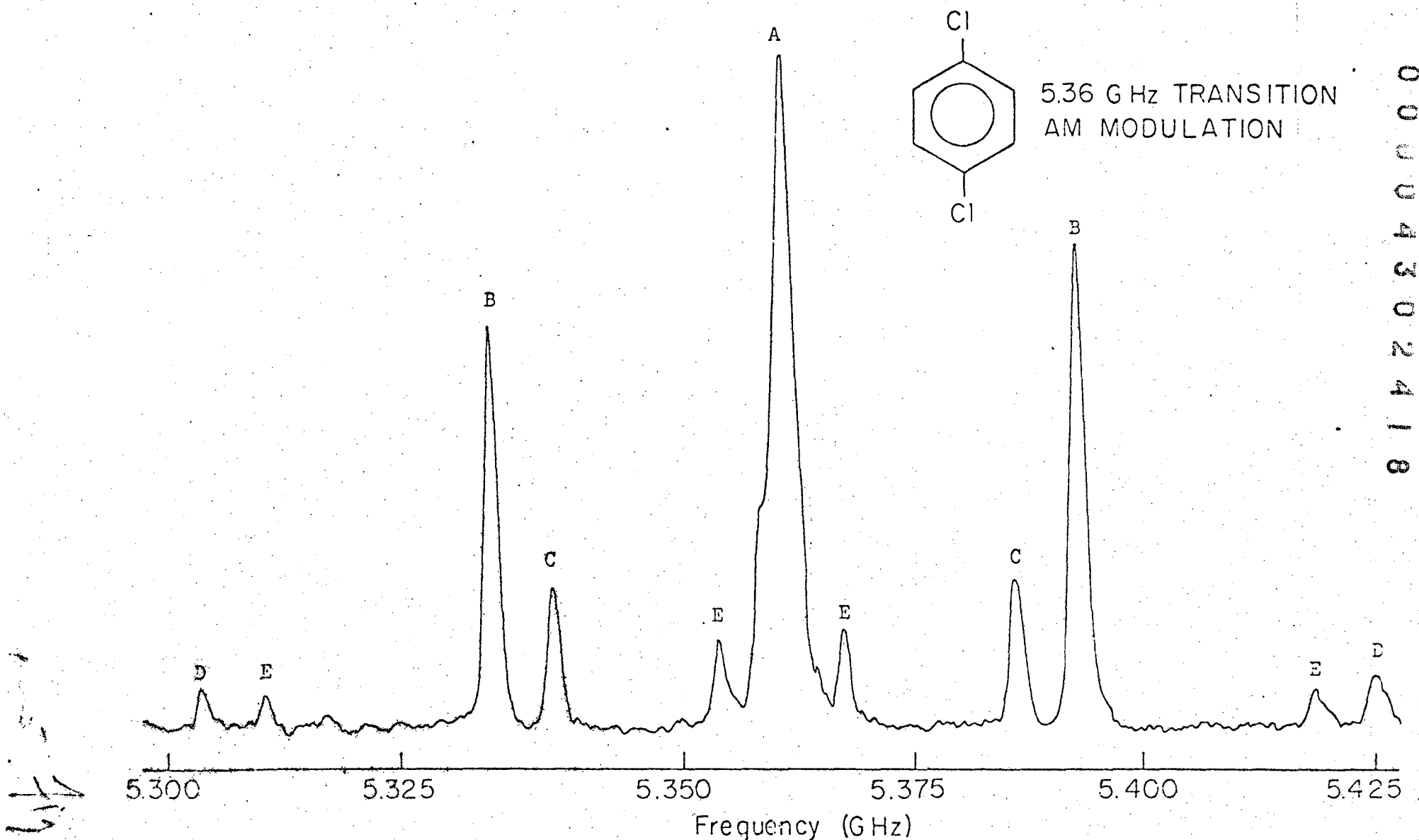
Cl
Cl
5.36 G Hz TRANSITION
AM MODULATION
A
B
B
C
C
D
D
E
E
E
E
5.300
5.325
5.350
5.375
5.400
5.425
Frequency (G Hz)

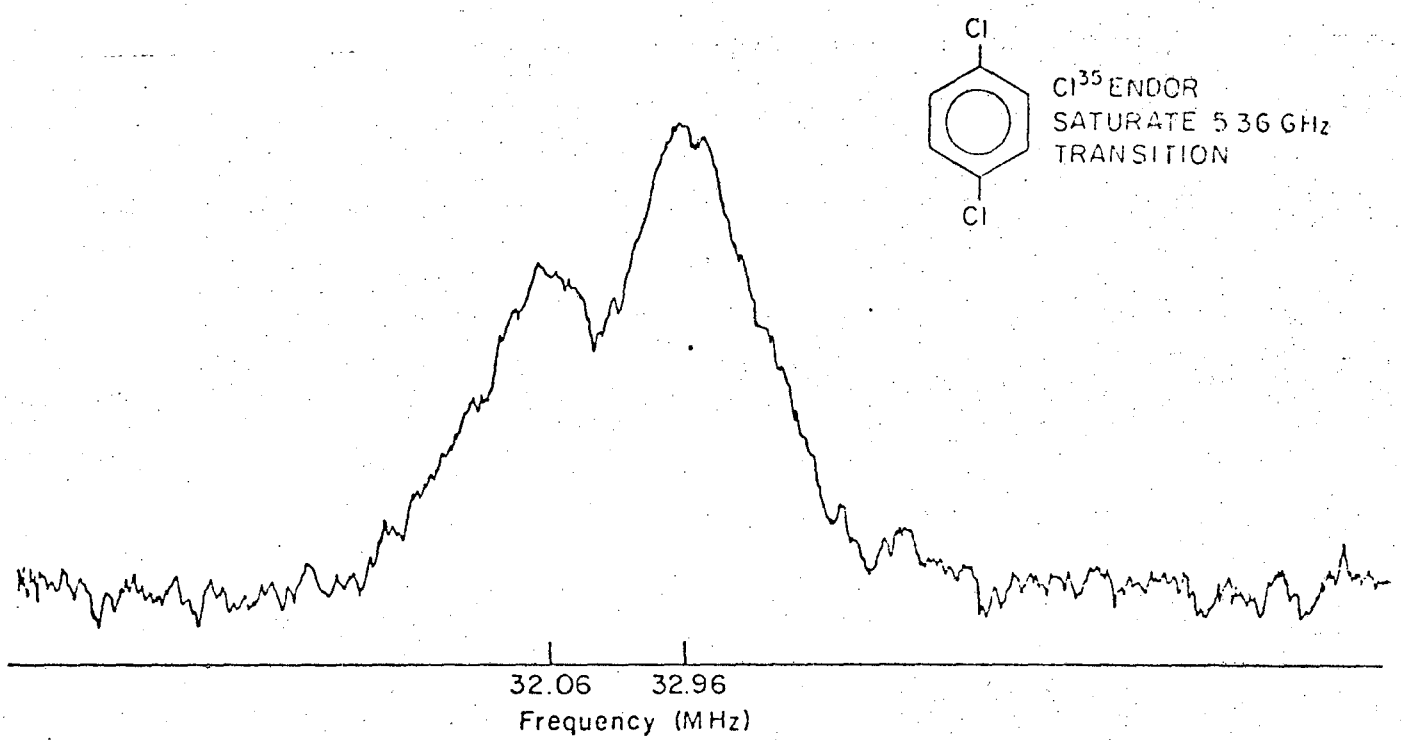


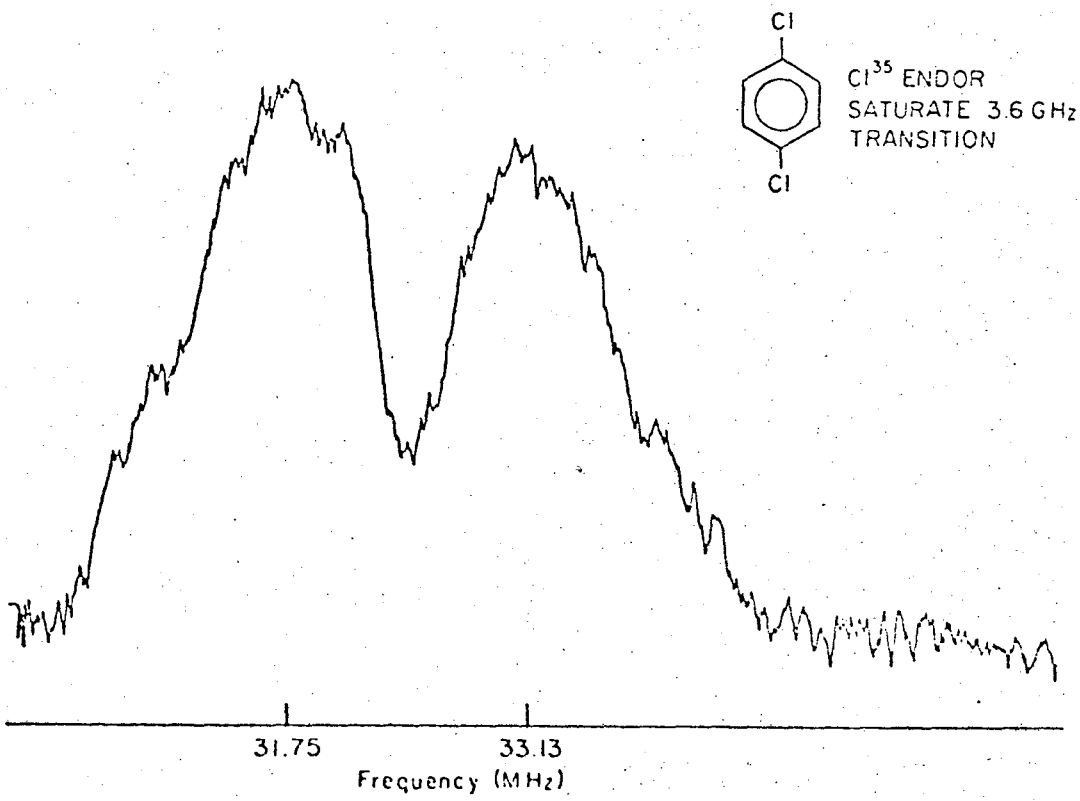


Fig 14

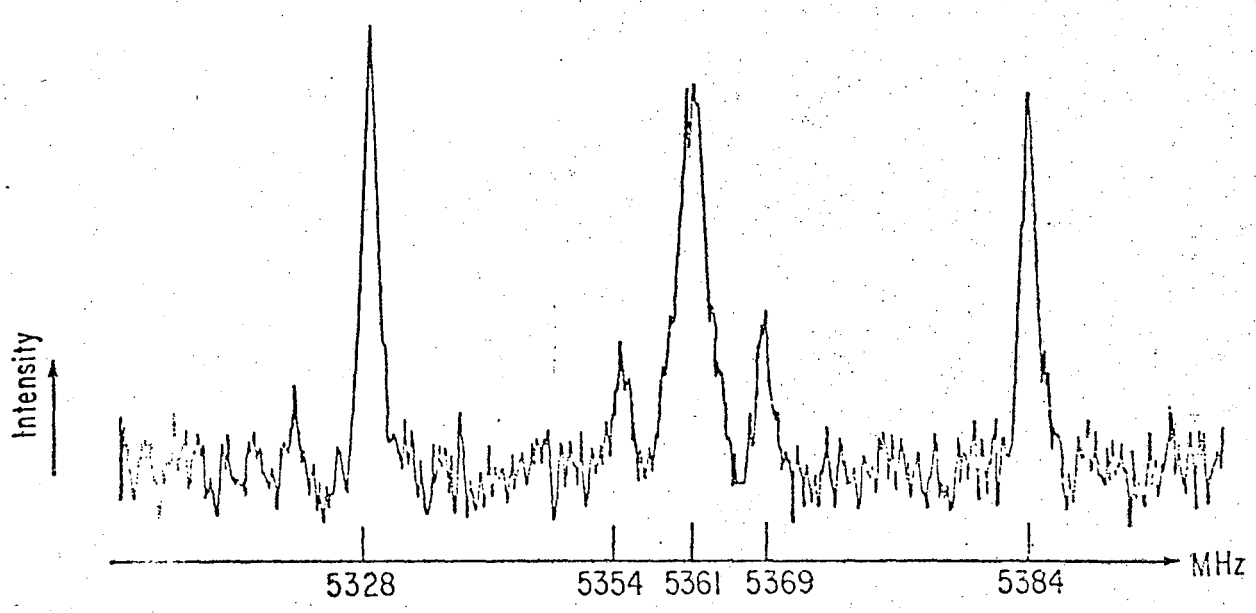


XBL 7012-7260

Fig 17

*TECHNICAL INFORMATION DIVISION*
*LAWRENCE BERKELEY LABORATORY*
*UNIVERSITY OF CALIFORNIA*
*BERKELEY, CALIFORNIA 94720*